UAB LIBRARIES
The University of Alabama at Birmingham

University of Alabama at Birmingham
UAB Digital Commons

All ETDs from UAB

UAB Theses & Dissertations

2018

Cerebral Vasospasm Detection And Treatment Using Transcranial Doppler Signal Analysis And Adaptive Medication Pump Mechanism

Khaled Elzaafarany
University of Alabama at Birmingham

Follow this and additional works at: https://digitalcommons.library.uab.edu/etd-collection

Recommended Citation

Elzaafarany, Khaled, "Cerebral Vasospasm Detection And Treatment Using Transcranial Doppler Signal Analysis And Adaptive Medication Pump Mechanism" (2018). *All ETDs from UAB*. 1597.
https://digitalcommons.library.uab.edu/etd-collection/1597

This content has been accepted for inclusion by an authorized administrator of the UAB Digital Commons, and is provided as a free open access item. All inquiries regarding this item or the UAB Digital Commons should be directed to the UAB Libraries Office of Scholarly Communication.

CEREBRAL VASOSPASM DETECTION AND TREATMENT USING TRANSCRANIAL DOPPLER SIGNAL ANALYSIS AND ADAPTIVE MEDICATION PUMP MECHANISM

by

KHALED ELZAAFARANY

ARIE NAKHMANI, COMMITTEE CHAIR
ABD ELMONIEUM NASER
EARL WELLS
KARTHIK LINGASUBRAMANIAN
MOUSTAFA HUSSEIN ALY

A DISSERTATION

Submitted to the graduate faculty of The University of Alabama at Birmingham,
in partial fulfillment of the requirements for the degree of
Doctor of Philosophy

BIRMINGHAM, ALABAMA

2018

CEREBRAL VASOSPASM DETECTION AND TREATMENT USING TRANSCRANIAL DOPPLER SIGNAL ANALYSIS AND ADAPTIVE MEDICATION PUMP MECHANISM

KHALED ELZAAFARANY

PHD IN COMPUTER ENGINEERING

ABSTRACT

In the United States, many patients pass away due to delayed detection of Cerebral Vasospasm (CV). Transcranial Doppler (TCD) is an efficient noninvasive, reliable device that can monitor the blood flow in various parts of the human brain like middle cerebral artery and basilar artery without any surgical intervention. It can help neurologists to diagnose many brain problems like edema, trauma, hemorrhage, and aneurysm. Unfortunately, continuous or even daily TCD monitoring is challenging due to the operator expertise and certification required in the form of a trained technologist, and certified physician to perform these studies. This barrier exists due to lack of automation for detection (without human intervention) of CV using TCD. To overcome this barrier, in this dissertation we present a timely, efficient novel algorithm that automates early detection of CV. We used the machine learning tools for CV detection, with the chosen time-frequency extracted features. Then we applied principal component analysis to reduce the data dimensionality. All the chosen features were used as input for training a decision-tree classifier. After that the CV detection model accuracy was evaluated with regard to noise robustness in real-time. The algorithm generated moderate accuracy. So, we enhanced the CV detection accuracy by adding continuous wavelet transform (CWT). The experimental results show 92.5% sensitivity for CV, and 95% specify for normal signals.

Subsequently, it is very important to establish a model for diagnosing and analyzing the abnormal cerebral blood flow velocity associated with CV. By generating such a model, it would be possible to design machine learning mechanisms for earlier prediction of CV. In the previous studies, cerebrovascular models of a blood flow behavior for different disorders were established. Unfortunately, those models are disease-specific and have too many parameters to tune. We have established a model for the signal envelope of the cerebral blood flow velocity that was produced by a transcranial Doppler. We have applied it to simulate CV behavior, but it is general enough to be applied to other cerebrovascular disorders. The model is based on the delay differential equations as a representative modeling equation for three cases: control (no CV or hyperemia), hyperemia, or CV. The model has only 4 tunable parameters and allows switching from one case to another by changing those parameters. After the validation of the model, the generated envelope signals were compared to recorded by transcranial Doppler spectrograms and demonstrated good match between the model and real signals in all three cases. This result could be used for modeling cerebral blood velocity abnormalities, early detection of CV, and potentially other disorders.

Finally, A syringe pump control system has been designed to supply an automatic process for flow control of medication. We have presented a device that injects certain amount of cc of drug into the patient in a prescribed time to handle the CV.

Keywords Cerebral Vasospasm, Transcranial Doppler, Machine Learning, Continuous Wavelet Transform, Delayed Differential equation, Cerebral Blood Flow Velocity.

ACKNOWLEDGMENTS

I would like to express my deep appreciation to Arie Nakhmani as my committee chair Professor and my mentor, who supports me and my research with great effort. Without his guidance and help, this dissertation would not have been generated.

I am especially indebted to Dr. Gyanendra Kumar, MD at the Neurology Department in the University of Alabama at Birmingham for supplying the transcranial Doppler datasets.

Nobody has been more important to me in the PhD dissertation than my family members. I would like to thank my parents; whose guidance and love are very essential in whatever I made in my life.

TABLE OF CONTENTS

Page

LIST OF TABLES

Table Page

LIST OF FIGURES

LIST OF ABBREVIATIONS

A-ARMA	adaptive auto regressive-moving average
ABP	arterial blood pressure
ANFIS	adaptive neuro-fuzzy inference system
AUC	area under the curve
AV	atrioventricular node
AWGN	additive white gaussian noise
BA	basilar artery
CBF	cerebral blood flow
CBFV	cerebral blood flow velocity
CFD	computational fluid dynamics
CPP	cerebral perfusion pressure
CV	cerebral vasospasm
CWT	continuous wavelet transforms
DCT	discrete cosine transforms
DDE	delayed differential equation
DIAS	Desmoteplase
EEG	electroencephalography

FDHMM	fuzzy discrete hidden Markova model
FFT	fast Fourier transform
HMM	hidden Markova model
HP	His-Purkinje node
ICP	intracranial pressure
IG	information gain
IIR	infinite impulse response
KNN	k-nearest neighbor
LMCA	right middle cerebral artery
MFCC	Mel frequency cepstral coefficients
MPC	model predicter controller
NEFCLASS	neuro-fuzzy classification
ODE	ordinary differential equation
PCA	principal component analysis
PI	pulsatility index
RBF	radial basis function
RMCA	right middle cerebral artery
ROC	receiver operating characteristic
SA	sinoatrial node

SNR	signal to noise ratio
SVM	support vector machine
TCD	transcranial doppler
WT	wavelet transform
ZCR	zero crossing ratio

CHAPTER 1

INTRODUCTION

Stroke (brain attack) is the third dominant disease that leads to death [1]. In the United States, each year approximately 140,000 people pass away from a stroke, 795,000 people experience complications from a stroke, and 185,000 people have repeated attacks [1]. A stroke takes place when cerebral hemodynamics (the difference between arterial and venous pressure) is stopped in any area of the brain [2]. Brain cells start to die due to lack of oxygen and the degree of ability to control muscle or memory disappears, which leads to weakness of arm (small stroke), partial or full disability, losing the capability to speak or death.

Besides that, a stroke can occur due to a limitation in blood flow. The blood circulates in the brain, delivers nutrients and oxygen to the brain cells, and removes waste; this cycle preserves the high rate of metabolism, which is important for the brain to work. A stroke can happen from vessel narrowing (Stenosis), clot formation (Thrombosis), blockage (Embolism), or blood vessel rupture (Hemorrhage).

Cerebral Vasospasm (CV) is one of the major causes of a stroke; it is a sudden contraction or decrease in diameter or flow rate of a blood vessel, which can affect tissue ischemia and tissue death (necrosis).

Aneurysmal subarachnoid hemorrhage patients face the common but feared complication of CV, which is evident in up to 70% patients angiographically and up to 80% sonographically [3] [4] [5].

The burden of silent CV is high with estimates of up to 60% [6]. Silent CV, left untreated, translates into cerebral ischemia and infarction in 20% [6]. Of patients that develop cerebral ischemia and infarction silently (asymptomatically), approximately 70% have Transcranial Doppler (TCD) evidence of vasospasm [6].

Vasospasm can be detected by angiography (dyes which X-ray can see, are inserted into blood vessels (either arteries or veins); the output pictures are called angiography), or by Doppler ultrasound signal from RMCA (right middle cerebral arterial), LMCA (left middle cerebral arterial) and BA (basilar artery) or integration of both.

The Middle Cerebral Artery is the main artery that causes a sudden stroke. This artery is supplying the lateral and frontal lobe with blood oxygen, that contains the primary motor and sensory areas of the face, throat, hand, arm and speech. On the contrary, basilar artery is supplying blood to the brain and central nervous system. The anatomy of these parts is shown in Figure 1.

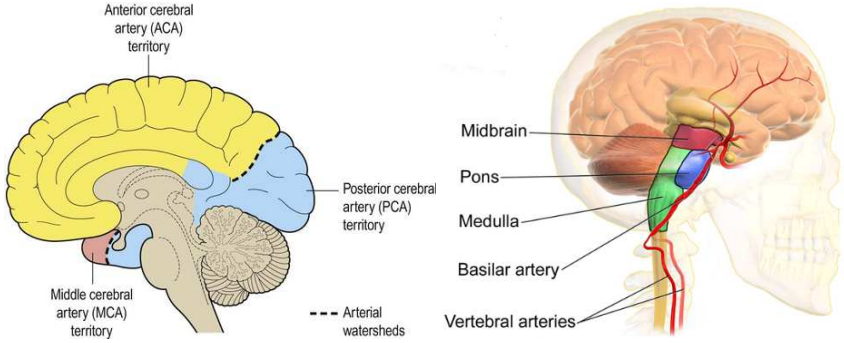

Figure 1 Middle Cerebral Artery Location in Human Brain [7], Basilar Artery Location in Human Brain [8].

Angiography is very expensive and not efficient device to monitor the CV with a real-time processing along the day when taking into consideration large number of patients and require continuous attendance of expert's physicians. Our collaborators have previously demonstrated that TCD evidence of vasospasm is predictive of delayed cerebral ischemia with high sensitivity (90%) and negative predictive value (92%), thus making it ideal for use in a monitoring device [9]. Due to its effective, safe, and noninvasive ability to detect cerebral vasospasm at the patient's bedside, it has been widely recommended by national guidelines for vasospasm surveillance in these patients [10] [11] [12]. Despite the obvious advantages of TCD monitoring over invasive angiographic methods for vasospasm detection, its use has not become commonplace in clinical practice. The prevalence of TCD monitoring among patients with aneurysmal hemorrhages is <2% in the nationwide inpatient sample [13]. A trained and certified technologist and interpretive expertise of a vascular neurologist are essential for diagnosis of CV in current medical practice. Continuous and daily TCD monitoring protocols can increase the yield of detection of CV. However, lack of automation for detection of CV, without human intervention, is a barrier to such clinical paradigms. We used the transcranial Doppler (TCD), and develop audio processing techniques for automatic distinguishing between CV, Hyperemia and control patients with alarming on CV in real-time. After CV detection an automatic control pump could be used for a treatment.

In this study, we will concentrate on TCD monitoring which is the type of Doppler ultrasonography that calculate the blood flow velocity through the blood vessels of the brain by measuring the echoes of ultrasound waves moving (through the windows in the skull). TCD is generally used to diagnose cerebral hemodynamics, stenosis, trauma,

aneurysm and hemorrhage [14]. The measurement of the brain blood flow rate requires advanced imaging processing techniques.

The TCD principle, based on measurement of the change in frequency of ultrasonic waves scattered from the moving blood cells, is used to calculate the blood flow velocity, utilizing what is known as the Doppler effect [15] The sound frequency increases as the source moves towards the receiver and decreases as it moves away from it. The Doppler shift $\mathbf{\Delta f}$ is given by the equation (1):

$$\mathbf{\Delta f} = \mathbf{2}\frac{\boldsymbol{v}}{\boldsymbol{c}}\mathbf{F}\cos\theta \qquad (1)$$

where $\mathbf{F}$ is the transmitted frequency, $\boldsymbol{v}$ is the blood velocity, θ is the beam-vessel angle and $\boldsymbol{c}$ is the sound speed in tissue.

TCD can detect the decrease or increase in blood flow rate or resistivity variation. There are two types of Doppler Ultrasonography: Pulsed-Wave Doppler and Continuous - Wave Doppler. The main different between the two kinds being that the continuous wave transducer has two elements, one for sending waves and another for receiving, while the pulsed wave transducer has just one element, which sends and receives signals [16].

Generally, the transmitted frequency is between 2 - 8 MHz and the velocity of blood in arteries is up to 5 or 6 m/s. That is used to form Doppler shift frequencies which are below 20 kHz inaudible band. Doppler ultrasound is especially used to measure velocity for moving blood.

However, due to vessel walls a high amplitude with low-frequency signals are generated, so it should have to be filtered out it by a high-pass filter, sometimes other moving things generate high amplitude signals which may distort the Doppler signal from

the blood. Air and bone can make high attenuation of Doppler signal. Doppler ultrasound signals from blood vessels can be calculated by using the appropriate equipment.

Nowadays the technique of transcranial Doppler has been sophisticated to enable Doppler signals to be measured from intracranial vessels. In this mechanism, some place of the skull like the squamous temporal bone is enough slim and regular to qualify passage beam of ultrasound without acute deformation.

In our work, we used a sound recording from ST3 Transcranial Doppler monitor for detecting Cerebral Vasospasm. There are two types; the first one is Bilateral, which has two channel TCD system with two diagnostic probes. Moreover, the other is Unilateral which has One channel TCD system with one diagnostic probe [17].

The monitor is shown in figure 2 (upper image), the bottom image is Marc 6oo Headframe. It is secure and comfortable, adjustable headframe available in either unilateral or bilateral configuration [17].

Figure 2 ST3 Transcranial Doppler and Marc 6oo Headframe *[17].*

Power M-mode program can simulate the velocity of blood in RMCA, LMCA, and BA with calculating its power, the number of samples, mean, DIAS (Desmoteplase (chemical compound) in Acute Stroke) and PI *(*pulsatility index *is calculated by* peak systolic velocity

- end diastolic velocity) / time averaged velocity*) can be* shown in Figure 3. After that, the recorded wave file is taken from TCD3 to MATLAB to apply signal processing on wave file and then to detect normal or vasospasm case.In the future, it would be desirable to predict vasospasm before it happens.

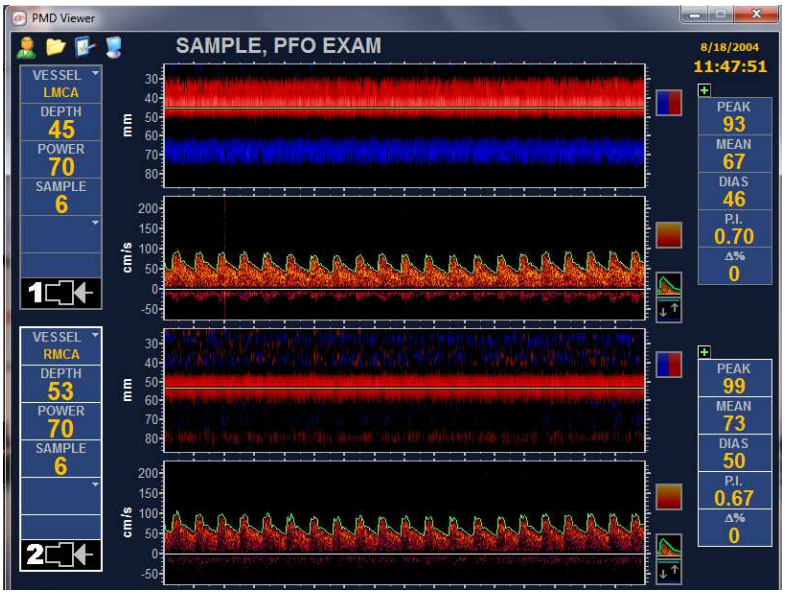

Figure 3 Power M-mode Doppler [17].

Literature Survey

We will discuss the different approaches or techniques for brain diseases detection using TCD. Two sources for such approaches could be considered. One is based on mathematical modeling of hemodynamic flow and using model parameters as features. Another approach is based on using audio analysis and classification features. Firstly, mathematical models of cerebral hemodynamics have been proposed by Ursino and Di Giammarco in 1991 [18]; Vasospasm is modeled, and it is shown that it affects only a single middle cerebral artery (MCA). In the first stage, the model is used to simulate some

clinical results reported concerning the patterns of MCA velocity, CBF *(*cerebral blood flow) and pressure losses during vasospasm. In the second stage, a correlation test is performed on model variables where a negative correlation between area and MCA velocity can be shown until CBF is well preserved. A positive correlation occurs when CBF starts to decrease significantly [18]. Arterial Blood Pressure (ABP) is the input; the outputs are Intracranial Pressure (ICP) and Cerebral Blood Flow Velocity (CBFV). The calculated outputs are subtracted to measure error [18]. Unfortunately, many variables in the model are unknown (could be predicted using available measurements), and this limits their use as classification features. The system is shown in figure 4. In other study, a nonlinear model with four features has been proposed to estimate CBFV as a function of arterial blood pressure [19]. Another work also investigated and compared CBFV to its spectral envelop features for classifying cognitive tasks [20].

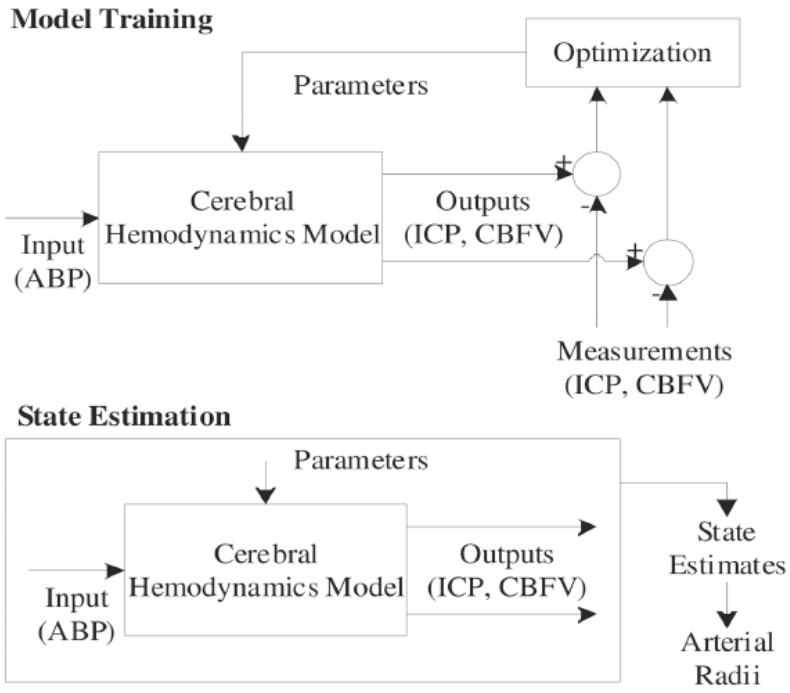

Figure 4 Model Training and State Estimation [18].

The second approach to TCD signal analysis is using frequency-time domain features. Nowadays, sound processing methods are well developed and widely used in our cell phones, smart watches, and computers. Though modern machine learning based algorithms could automatically transcribe music and recognize speech, those algorithms were not explored enough about their applicability in medical diagnostics. The physicians still rely on their experience and senses to diagnose various diseases instead of using automated techniques. However, sound analysis and machine learning start to take their place in medicine. Multiple works have investigated the possibility of TCD application to detection of various brain conditions using time and frequency domain methods. For example, fast Fourier Transform (FFT), wavelet transform (WT) and adaptive autoregressive moving average (A-ARMA) methods have been applied by Guler et al. to TCD signals which recorded from the middle cerebral artery to obtain TCD frequencies [21] and for spectral image analysis of TCD signal. From the spectral resolution of TCD signals, doppler frequency is measured, where various vessel diseases can be discovered by maximum frequency curves (sonogram envelope). Besides that, the resistive index can be used to find the cerebral pressure. The results shows, A-ARMA produced the best spectral resolution than FFT and WT [21].

The choice of a classifier and data dimension reduction technique play a significant role in getting robust results. Ozturka and Arslanb performed the chaos analysis on the transcranial Doppler (TCD) signals recorded from the temporal region, two chaotic invariant measures were calculated, i.e. the maximum Lyapunov exponent and the correlation dimension. They used them for automatically differentiating various cerebrovascular conditions via classifiers. Several different classification algorithms were

investigated; the k-nearest neighbor algorithm outperformed all the other classifiers with a classification accuracy of 94.44%. The receiver operating characteristic curves (ROC) were used to assess the performance of the classifiers [22]. The result was that these classification systems which use chaotic invariant measures as input to classifier can detect the blood flow velocity changes in different diseases.

However, Uguz aimed to classify the TCD signals by using information gain (IG) as a feature ranking and principal component analysis (PCA) as dimension reduction to improve the classification efficiency and accuracy. The ranked feature is sorted in a decreasing order according to its importance with various ratios (10–100%). Then in PCA technique, the low importance features were ignored, and the high importance features were selected Then, the PCA method experiments were conducted using a support vector machine (SVM) classifier [23]. The most important stage in applied PCA is how to measure the number of principal components. The p number of principal components to be chosen among all principal components should represent the data at their very best. In this study, the cumulative percentage of variance criteria, for its simplicity and acceptable performance, was applied to determine the number of principal components [24]. The broken-stick model, Felicia's partial correlation procedure, cross-validation, Barlett's test for equality of Eigenvalues, Kaiser's criterion, Cattell's screen-test, and the cumulative percentage of variance are a few of such criteria [24] [25].

When KNN classification is implemented, the most important variable affecting classification is a k-nearest neighbor number. Usually, the typical k value is empirically determined to achieve the lowest classification error ($k = 5$ was determined). Besides that, Euclidean distance is used as the distance metric.

By using C4.5 decision tree algorithms, in the pruning phase, the post-pruning method is used to take the decision when to stop expanding a decision tree. The confidence factor is used for pruning the tree. In this study, the confidence factor is assigned as 0.25. The pruned trees consist of 8 leaves and 12 nodes.

The SVM classifier efficiency hugely depends on the choice of kernels. There are many kinds of kernels such as the radial basis function (RBF) kernel, polynomial kernel, and B-spline kernel. However, there are no well-established theories to select kernel functions [26]. Where the RBF kernel, which is one of the most popular kernel functions, is used, the classification efficiency is examined by using statistical parameters like sensitivity, specificity, areas under the ROC curves (AUC) and standard error; an SVM-based classifier gives a better result than KNN and C4.5 decision tree classifiers.

Also, adaptive neuro-fuzzy inference system showed promising results [27]. TCD signals were classified by Ozturk et al. by using neuro-fuzzy classifier of the non-stationary chaotic invariant TCD signal [27]. A chaos analysis of the TCD signals recorded from the middle arteries of the temporal region, found that all of the TCD signals represented nonlinear dynamics and had an underlying low-level determinism. The maximum Lyapunov exponent ($\boldsymbol{\lambda}$), which is the strongest quantitative indicator of chaos, was found to be positive for all TCD signals, but the correlation dimension (D2) was found as greater than 2 and as a fractional value for all TCD signals. This result indicates that the nonlinear dynamics of the TCD signals corresponds to a strange attractor in phase space. The ANFIS (Adaptive Neuro-Fuzzy Inference System) model fulfilled better percentage in classification accuracy than the NEFCLASS (Neuro fuzzy classification) model. The classification accuracy of the ANFIS model after training was 94.40% whilst this value

was found as 88.88% for the NEFCLASS model [27]. The proposed classification systems with chaotic invariant features, were able to detect the CBFV changes in different disorders [22] [27]. Uguz proposed the Rocchio-based hidden Markov model(HMM) and fuzzy discrete hidden Markov model (FDHMM) for enhancing the classifications of TCD signals [28] [29].

Recent advances in extracranial Doppler studies have also contributed to improving the tools for vasospasm detection. Ryu et al. [30] developed a numerical model that was used to measure the extracranial blood velocity in anterior and posterior vasculature to detect vasospasm. The authors demonstrated the velocity ratio in carotid and vertebral arteries to identify severe vasospasm (impaired cerebral autoregulation) using noninvasive extracranial Doppler, which also can detect the changes in blood pressure and cardiac output [30].

As seen in many studies, Fourier transform and integral transforms are used widely, but the techniques cannot display time and frequency information details that would be sufficient for a good classification to detect many diseases. This means that many features of interest will be lost during the processing due to poor spectrum resolution especially in different noise power of non-stationary signals. Therefore, we tried to use both time and frequency features for classification with using the wavelets features to enhancing feature extraction method because it gives optimal time-frequency resolution in all ranges of frequencies. The major advantage of the wavelet transform is that the window size can be varied for low and high frequencies. For this benefit, the wavelet transform is applied in image processing [31] [32], signal processing [33] [34] and biomedicine [35]. The results were compared with the physician's decision for verification of the proposed work and

then, the extracted model is tested at different noise power. Internal or external noise to the signal will cause appearance of a new or extra frequency which can influence the estimation detection of neurology problems.

The second part of our study is CV modelling. Previous studies showed significant relationship between the hemodynamics of cerebral vessels and the cerebrovascular diseases [36] [37]. Cerebral hemodynamics can be monitored or measured using the cerebral blood flow velocity (CBFV) [38] [39]. The TCD ultrasonography device measures the blood flow rate by calculating the difference between the transmitted ultrasound and its returned echo. The CBFV is measured from left or right middle cerebral artery (LMCA, RMCA), or Basial Artery (BA). The accuracy of analyzing and modeling are very important for early detection and prediction of the occurrence of cerebrovascular disorders.

Unfortunately, there is no simple, reliable and easily tunable mathematical model of CBFV. Olufsen established the cerebral artery blood flow velocity curve by using the resistors and a capacitor of Windkessel with taking into consideration the arterial pressure changes [40]. Ursino et al. modelled the cerebral blood flow regulation which comes from the superimposition and interaction of several concomitant effects [41]. In other studies, a computational fluid dynamics (CFD) approach was used to model and monitor the CBFV [42] [43]. More recently, Liu et al. suggested purely mathematical modeling approach (instead of biologically or physically inspired) by using the eight's order Fourier series to fit to the cerebral perfusion pressure of the CBFV graphs [44] [45]. Panunzi et al. proposed the five Stochastic Delay Differential Equations (SDDEs) that can generate the aterial pressure and CBFV [46]. Therefore, it is very important to try to create a mathematical

model for all this CBFV in different cases. From this point of view, the overall goal of the second part of PhD is to use sophisticated mathematical model to simulate the brain problem waves and compare them with the real TCD recordings. We adapted the Delayed Differential Equation (DDE) of the cardiac electrophysiology model to model the CBFV of the brain and compare the model output with the real TCD waves output. The objective was to obtain the better model with less parameters than offered in the previous studies. The effective range of parameters for CV, hyperemia and control participants was computed.

The third part of the study is to present an algorithm for medication controlling along the pump to automatic CV treatment. There is a study that presents an algorithm for controlling glucose in the blood using a closed-loop insulin infusion pump, where the controller is designed from the 19^{th} order of human glucose-insulin system. The results give 40% improvement in overshoot and 23% decrease in settling time. In the simulation, the linear model predictive controller(MPC) outperformed other suggested closed-loop algorithms [47]. By incorporating state estimation, further improvement in controller performance was realized. The state estimating controller is robust to patient-model mismatch. Where glucose and insulin dynamics are represented by three differential equations, two are physiologic, and the remaining four are used for fitting patient data.

In another study, a nonlinear model predictive controller was presented to keep normoglycemia in patient with type 1 diabetes during fasting and overnight fast. The controller uses Bayesian parameter estimation to determine time-varying model parameters. The model predictive has been evaluated using data from 15 clinical experiments in patient with type 1 diabetes [48].

In another study, a closed-loop insulin infusion pump is developed to maintain a normoglycemia in type I diabetic. Filtering the impulse response coefficients via projection onto the Laguerre basis is used for linear identification of an input-output model from noisy data of the patient. A linear model predictive controller is presented using the identified step response model. Glucose setpoint tracking performance is enhanced by designing a second controller which substitutes a more detailed internal model containing state-estimation and a Kalman filter for the input–output representation. The state estimating controller maintains glucose 15 mg/dl of the setpoint in the occurrence of measurement noise. Under noise-free conditions, the MPC with state estimation outperforms an internal model controller (49.4% reduction in undershooting and 45.7% decrease in settling time). These results demonstrate the potential use of predictive algorithms for blood glucose control in an insulin infusion pump [49].

In the following chapter, the framework or structure of the methods and techniques of TCD signal processing are presented with using machine learning tool for medical diagnostics. Then the mathematical modelling of TCD signals are presented in the same chapter. In the results chapter, we demonstrate the application of the framework to detection of CV in stroke patients taking into consideration the effect of noise on the dataset and the performance of the different SNR and comparing the results of the created DDEs model with TCD orignal signals. Finally, the conclusion chapter summarizes our studies and proposes the future research directions.

CHAPTER 2

RESEARCH METHODOLOGY

There is a direct analogy between speech and music analysis and other kind of sound analysis (Doppler). Doppler sound could be explored using developed for speech and music tools/features. We applied the speech, sound, and music analysis approaches to the Doppler sound to detect and classify various brain disorders or events. The audio signal is acquired with TCD and analyzed for further classification. The signals are recorded, or processed directly from the audio output of the TCD. Figure 5 shows one example of the cerebral vasospasm (bottom) signal and normal (top) TCD signal at the same time and voltage scale. It is visually obvious that those two signals are different, but it is not obvious how this difference could be quantified. In addition, in many cases normal and abnormal signals are very similar in their appearance. The framework consists of two main stages:

1) TCD-Data Collection
2) TCD-Data Classification

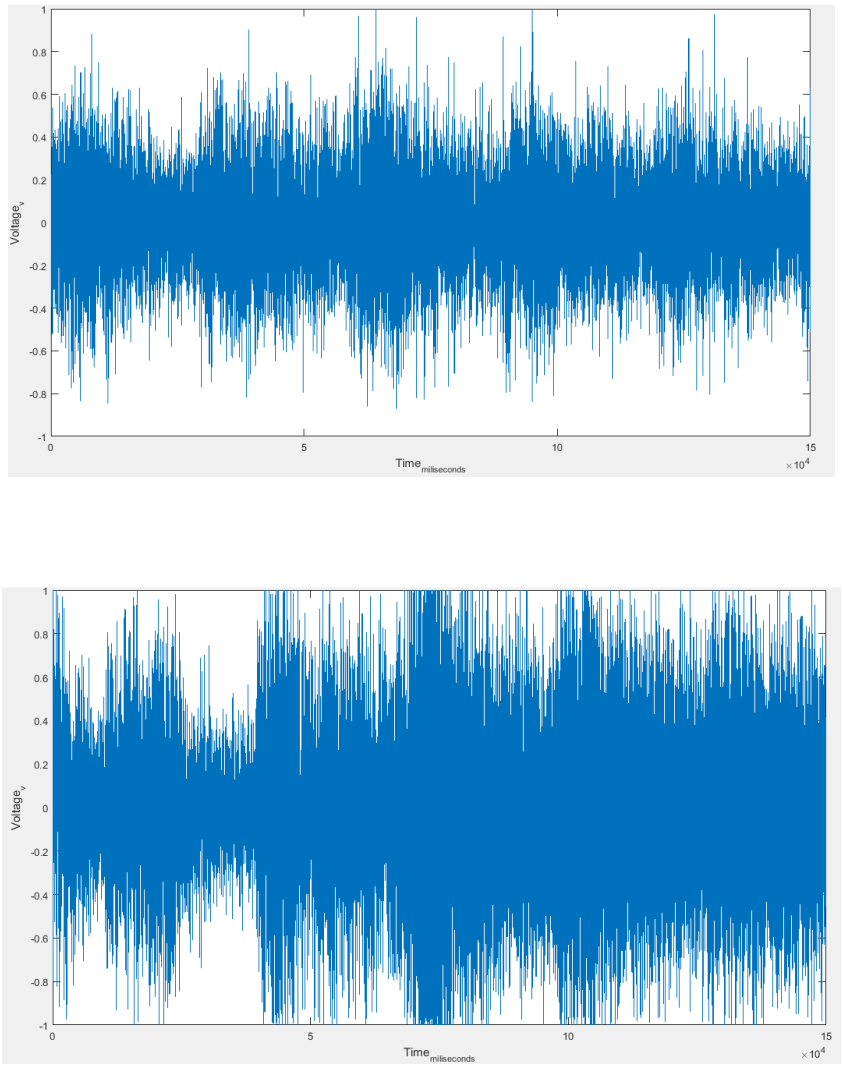

Figure 5 TCD Recording from Control (top) and Cerebral Vasospasm (bottom) Cases.

TCD-Data Collection

In this study, 160 TCD audio database were recorded from 16 subjects of 3 seconds duration with sampling rate 44.1kHz. The signals were recorded once a day for 5 days on average. All methods were carried out in accordance with relevant guidelines and regulations, 160 Doppler audio signals were retrospectively recorded from existing TCDs on proximal arterial segments of the left middle cerebral artery and right middle cerebral artery from patients in an IRB approved aneurysmal subarachnoid hemorrhage registry

(University of Alabama at Birmingham Institutional Review Board Protocol Number: X150622004). Informed consent was not required for retrospective analysis of de-identified Doppler audio data. The signals were classified manually by a vascular neurologist as CV or normal (without CV). There were 8 normal subjects and 8 CV subjects had detected in RMCA, LMCA, or both. All of them were transferred from TCD to the PC by an auxiliary audio cable.

TCD-Data Classification

The problem of CV identification could be formulated as a pattern recognition problem. For framing CV detection as a pattern recognition problem, we used training based on manually classified cases of CV. Four steps are applied on the dataset to detect the CV subjects. The first is feature extraction, dimension reduction, feature scaling and mean normalization then the classifier. All the results are compared with the decision of vascular neurologist. Finally, to enhance the sensitivity and specificity percentage, we used the CWT.

Feature Extraction

A Feature extraction is an essential step in pattern recognition. It commonly used in machine learning and audio signal processing to compress the big dataset size or the redundancy information [50] into small size and at the same time to increase the classifier efficiency. There is an infinite number of ways to define features; we have carefully selected from the features used in audio research those that might be useful in TCD analysis and beyond. We used features from time and frequency domains to analyze audio signals. The time domain features are zero-cross rate (ZCR), energy, and energy entropy. We

combined them with more advanced frequency domain features like 13 Mel-frequency cepstral coefficients (MFCC), 12 Chroma coefficients, spectral centroid, spread, entropy, spectral roll-off, spectral flux and harmonic ratio for periodic estimation. They were extracted directly from the sampled audio files. We displayed the effect of each of these 12 features on the CV detection in the wavelet section.

Zero-Crossing Rate

ZCR used as a feature in the narrowband signals and audio analysis [51]. It reflects or count the number of times the waveform changes its algebric sign during the frame per second [52]. The average rate can be used as a feature in the classifier input and it can be used as a feature in audio analysis [51].

$$Z(i)=\frac{1}{2S}\sum_{n=1}^{S}|sign[x_i(n)]-sign[x_i(n-1)]| \qquad (1)$$

$$s_i(n)]=\begin{cases}+1 & x_i(n)\geq 0\\ -1 & x_i(n)<0\end{cases} \qquad (2)$$

Harmonic Ratio

Any audio signal can be classified as quasiperiodic or aperiodic. For simplicity, We classified the TCD signals as quasiperiodic in order to predict the fundamental period by using the autocorrelation function [53]. The first step was shifting the signal and calculating the correlation of the original signal with the shifted one. Then the maximum autocorrelation was chosen [54]. The autocorrelation function for frame *i* is given by:

$$R_i(m)=\sum_{n=1}^{S}x_i(n)\,x_i(n-m) \qquad (3)$$

In the second step we normalized the autocorrelation function and taking the max to get the harmonic ratio:

$$\mathrm{Max}(N_i(m)) = \frac{R_i(m)}{\sqrt{\sum_{n=1}^{S} x_i(n)^2 x_i(n-m)^2}} \quad (4)$$

Energy

Energy is frequently used in audio content analysis [55]. The training set of audio files was divided into sequences of frames, each frame was divided into samples, and then square absolute summation of the frame samples was performed to obtain each frame's energy [56], which is shown in equation (2):

$$E(i) = \sum_{n=1}^{S} |x_i(n)|^2 \quad (5)$$

where $x_i(n)$ is the audio samples of ith frame, and S is the number of samples in the frame. We normalized every output of frame energy by dividing $E(i)$ by S to compute the power of the signal [56]. The equation for power computation is:

$$P(i) = \frac{1}{S} \sum_{n=1}^{S} |x_i(n)|^2 \quad (6)$$

Energy Entropy

This feature is used for the determining the sudden variations in the level of energy in the audio signal [56] [57], it measured my dividing each wave file into frames, then dividing the energy of each frame (E_i) in energies of sub-frame (E_k where k from 1 to P) of the same duration, then normalized by the energy of the frame [58].

$$E_i = \sum_{k=1}^{p} E_k \quad (7)$$

$$E_{\mathrm{n}} = \frac{E_k}{E_i} \quad (8)$$

The energy entropy is defined by:

$$H(i) = -\sum_{n=1}^{p} E_{\mathrm{n}} * \ log_2(E_{\mathrm{n}}) \quad (9)$$

Mel-Frequency Cepstral Coefficients

MFCC is defined as the short time speech spectrum, it used mainly in the field of speech processing [59] in the application of human speech prediction [60] [61] and it can be used in music. It reflects the representation of signal cepstral, where after measuring the log-amplitude of the power spectrum of nonlinear Mel frequency, the FFT bins were graded and smoothed per the perceptually motivated Mel-frequency scaling. Finally, discrete cosine transforms (DCT) was performed to decorrelate the resulting feature vectors [62], [51] Although we tested 13 coefficients for CV detection, we found that performance of the first coefficient was the best for classification.

Chroma

The Chroma vector is a 12-element representation of the spectral energy as proposed by Wakefield [63]. These features are frequently used in music applications [64] [65]. and widely used to predict the music that produced from piano. The Chroma vector was calculated by converting the DFT coefficients of a signal into 12 bins. Each bin represents one of the 12 equal tempered pitch classes. Each bin generates the mean of log-magnitudes of the DFT coefficients. [56] We found that the first and second coefficients gave the best classification performance:

$$v_k = \sum_{k=1}^{n} \frac{X_i(n)}{N_k} \quad (10)$$

Spectral Entropy

It used for music [66] and speech discrimination. The spectral entropy [57] is calculated similarly to the entropy of energy, but it is computed in the frequency domain and so we divided the spectrum of the frame to sub-bands energy E_b, where b= 0, 1,… L-1, then normalized by the energy of spectrum frame.

$$H = -\sum_{b=0}^{L-1} \frac{E_b}{\sum_{b=0}^{L-1} E_b} * log_2\left(\frac{E_b}{\sum_{b=0}^{L-1} E_b}\right) \quad (11)$$

Spectral Centroid

It used for music, speech discrimination and watermarking [67] [68] and used for speech and music discrimination [67]. The spectral centroid is defined as mass center of the spectrum. The spectral centroid value C_i of the *i*th audio frame, is defined as:

$$C_i = \frac{\sum_{k=1}^{f} k \,.\, X_i(k)}{\sum_{k=1}^{f} X_i(k)} \quad (12)$$

where $X_i(k)$, $(k = 1, \dots, f)$ are the magnitudes of discrete Fourier transform coefficients of ith frame.

Spectral Spread

It used for music, speech discrimination and watermarking [67], [68]. The spectral spread is the second central moment of the spectral centroid. We calculated it by finding the deviation of the spectrum from the spectral centroid, according to the following equation [56]:

$$S_i = \sqrt{\frac{\sum_{k=1}^{f}(k-C_i)^2 X_i(k)}{\sum_{k=1}^{f} X_i(k)}} \quad (13)$$

The spectral spread is used to monitor spectral shape, and is generally used in watermarking of audio signals [68].

Spectral Roll-off

Spectral roll-off is used to discriminate between the voiced and unvoiced signal [54], but we used it as feature extraction in CV detection. It is defined as the 95th percentile of the power spectral distribution (R_t) [51].

$$\sum_{k=1}^{R_t} X_i(k) = 0.95 * \sum_{k=1}^{f} X_i(k) \quad (14)$$

Spectral Flux

Spectral flux calculates the spectral deviation between two consecutive frames and was measured as the squared difference between the magnitudes of the spectra of two consecutive windows [51]:

$$F_i = \sum_{k=1}^{f}(N_i(k) - N_{i-1}(k))^2 \quad (15)$$

where $N_i(K)$ is the normalized magnitude of Fourier transform of the current frame.

Dimension Reduction

This step was used after the feature extraction, because the extracted features may be correlated, or have redundant information, which can lead to decreasing efficiency of the classifier used. Principal Component Analysis (PCA) or Karhunen-Loeve is applied in dimension reduction processes in the pattern recognition [69] for feature generation, it

mapping the original space to a lower dimensional one using a mathematical transformation [59] [70]. PCA is a statistical process that converts certainly correlated variables to linearly uncorrelated variables, which are called principal components. Furthermore, the number of principal components needed to sufficiently describe the original data is generally smaller than the original data. The first principal component has the highest variance and all output vectors should be orthogonal. In our research, we used the PCA technique of the wave file as an array with 99% variance, in order to increase the classifier efficiency.

Feature Scaling and Mean Normalization

Feature scaling is used to standardize the values of independent variables or features of the dataset [71]. In data processing, it is known as data normalization and is performed during the data preprocessing step before classifier. Since the values of raw data are varied widely, the normalization is necessary. We applied feature scaling for the twelve features before extracting the classifier model. Another reason for using feature scaling is a faster convergence of gradient descent algorithm which is used in the training process [72]. After normalization, all feature values were distributed between 1 and -1.

Classification

In the fourth stage, all features were fed to different classifiers. The trained classifier arrives to the decision about the problem. Various CV classifying techniques were tested, e.g., Decision Trees, K-Nearest-Neighbors, Discriminant Analysis, Logistic Regression, and Support Vector Machines. We found that ensemble bagged decision tree classifier gives the highest classifcation accuracy. It uses a flowchart where each node has a true/false

test; each branch shows the output of a trial. The classification law is the path from the output(root) to the input (leaf), so it could be implemented by "if" condition statements. The framework is providing supervised training of the classifier offline.

Alternative approach in other study, uses zero crossing density, spectral centroid, and median of Welch spectrum estimator as feature extraction and cross-validation to compare the performances of different predictive modeling; it achieved 82% accuracy.

Continuous wavelets transform (CWT)

It used for time-frequency analysis tool for non-stationary signals; wavelet can give us long time interval and short time interval for the low-frequency band and high ones [73] [74]. So, it can provide many frequency information details at low frequency and many time information detail at low frequency. The wavelet transform can be applied to discrete- and continuous-time signals. In this study, the continuous wavelet transform gives better results. CWT enhance the sensitivity and specificity percentage compared to that published in [75].

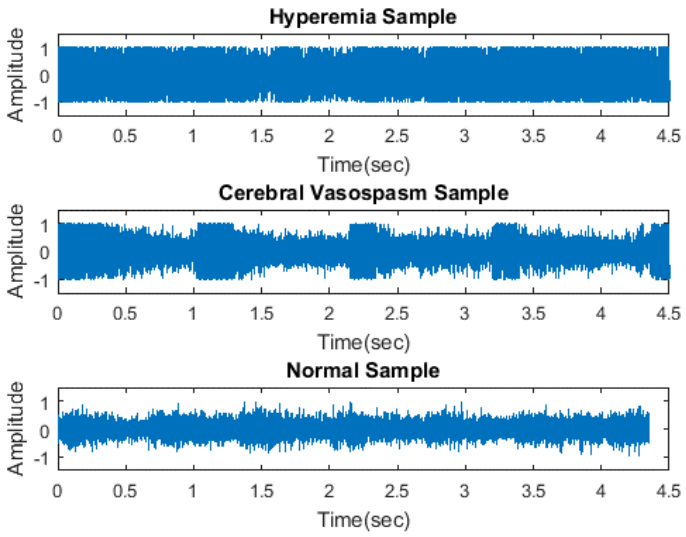

Figure 6 The Time Domain of the TCD Wave Files for Normal, Hyperermia and CV Cases.

Figure 6 shows the difference between TCD signals in time domain for the three cases after transferring the signal from TCD device to the MATLAB by auxiliary cable. Unfortunately, the visual differences are not consistent and difficult to quantify.

After recording the TCD wave files from the MCA and transferring them into frequency domain, the three CBFV cases can be considered as periodic signals. Based on our experiments, there is a high similarity between the TCD signal and the heart electrophysiological model (PQRST) especially the ST interval described in [76]. ST interval period (starts from the end of the QRS-interval to T-wave) are corresponding repolarization process in ventricular heart chamber. The cardiac conduction system can be synthesized by three self-excited pacemakers. Sinoatrial (SA) node is the dominant pacemaker of the cardiac and having the highest intrinsic rate [76] [77] [78]. Other pacemakers like atrioventricular (AV) node and the His-Purkinje system (HP) have low intrinsic rate [76] [77] [78]. we can model the heart conduction physiology system by using two-coupled nonlinear oscillators.

$$\dot{x}_1 = \frac{1}{C_{SA}} x_2 \tag{16}$$

$$\dot{x}_2 = -\frac{1}{L_{SA}} [x_1 + f_1(x_2) + R(x_2 + x_4)] \tag{17}$$

$$\dot{x}_3 = \frac{1}{C_{AV}} x_4 \tag{18}$$

$$\dot{x}_4 = -\frac{1}{L_{AV}} [x_3 + f_2(x_4) + R(x_2 + x_4)] \tag{19}$$

Where the parameters C_{SA}, L_{SA}, C_{AV}, L_{AV}, R can be obtained experimentally and they reflected the physiological properties of heart conduction system. The functions f_1 *and* f_2 are voltage sources depending on currents x_1 and x_2 respectively, but this did generate the PQRST interval well and TCD signal.

Other approach used the Van de Pol (VdP) ordinary differential equation (ODE) to model the cardiac pacemaker. The VdP system is used to displays the characteristic behaviors in physiological system that contains limit cycles, complex periodicity, synchronization and chaotic dynamics [79] [80].

As already mentioned, the normal cardiac rhythm is mainly produced from the SA node, which can be known as the normal pacemaker. Each depolarization followed by repolarization in different region of the heart which generate currents with different magnitudes. Therefore, the combination of different activations waves from each heart region is responsible for the PQRST wave form. Under these assumptions, it is found that the coupled oscillators can represent the general heart beat dynamics and TCD signal. Usually two oscillators can generate similar signal as the SA and AV nodes. But, these two oscillators cannot produce PQRST wave in the right form like ECG output. This is because

the signal from the first oscillator is used for the SA node and atrium polarization and the signal from the second oscillator for the ventricle depolarization. So, it is possible to generate the P-curve but not the QRS complex [81].

$$\dot{x}_1 = x_2 \tag{20}$$

$$\dot{x}_2 = K(x_1 - w_1)(x_1 - w_2)x_2 - b_1 x_1 + c_1(x_3 - x_1) + a_1 \sin(w_1 t) \tag{21}$$

$$\dot{x}_3 = x_4 \tag{22}$$

$$\dot{x}_4 = k(x_3 - w_1)(x_3 - w_2)x_4 - b_2 x_3 + c_2(x_1 - x_3) \tag{23}$$

Where $x_1,\ x_2\ for\ SA\ node\ and\ x_3,\ x_4$ for AV nodes [82], and model parameters ($K, w_1,$ $w_2, b_1, b_2, a_1,\ c_1, c_2$) are obtained experimentally. This observation conclude that we should use the third oscillator which physiologically generates the His–Purkinje complex. This conceptual model may be represented by a set of differential equations as follows [83]:

$$\dot{x}_1 = x_2 \tag{24}$$

$$\dot{x}_2 = -a_{SA} x_2 (x_1 - w_{SA1})(x_1 - w_{SA2}) - x_1(x_1 + d_{SA})(x_1 + e_{SA}) + \rho_{SA} \sin(w_{SA} t) - K_{SA-AV}(x_1 - x_3 - K_{SA-HP}(x_1 - x_5) + u_1 \tag{25}$$

$$\dot{x}_3 = x_4 \tag{26}$$

$$\dot{x}_4 = -a_{AV} x_4 (x_3 - w_{AV1})(x_3 - w_{AV2}) - x_3(x_3 + d_{AV})(x_3 + e_{AV}) + \rho_{AV} \sin(w_{AV} t) - K_{AV-SA}(x_3 - x_1 - K_{AV-HP}(x_3 - x_5) u_2 \tag{27}$$

$$\dot{x}_5 = x_6 \tag{28}$$

$$\dot{x}_6 = -a_{HP}x_6(x_5 - w_{HP1})(x_5 - w_{HP2}) - x_5(x_5 + d_{HP})(x_5 + e_{HP}) +$$
$$\rho_{HP}\sin(w_{HP}t) - K_{HP-SA}(x_5 - x_1) - K_{HP-AV}(x_5 - x_3) + u_3 \quad (29)$$

Time delayed in the signal are used to change the coupled oscillators conduction. The adding of time delays in differential equations can make a severe change and generate chaos emerges in a system that can be defined as a regular behavior [84] [85] [86]. On this assumption, the delayed differential equation can be written as [84]:

$$\dot{x}_1 = x_2 \quad (30)$$

$$\dot{x}_2 = -a_{SA}x_2(x_1 - w_{SA1})(x_1 - w_{SA2}) - x_1(x_1 + d_{SA})(x_1 + e_{SA}) + \quad \rho_{SA}\sin(w_{SA}t) -$$
$$K_{SA-AV}(x_1 - {x_3}^{T_{dSA-AV}} - K_{SA-HP}(x_1 - {x_5}^{T_{dSA-HP}}) + u_1 \quad (16)$$

$$\dot{x}_3 = x_4 \quad (31)$$

$$\dot{x}_4 = -a_{AV}x_4(x_3 - w_{AV1})(x_3 - w_{AV2}) - x_3(x_3 + d_{AV})(x_3 + e_{AV}) + \quad \rho_{AV}\sin(w_{AV}t) -$$
$$K_{AV-SA}(x_3 - {x_1}^{T_{dAV-SA}} - K_{AV-HP}(x_3 - {x_5}^{T_{dAV-HP}})u_2 \quad (18)$$

$$\dot{x}_5 = x_6 \quad (32)$$

$$\dot{x}_6 = -a_{HP}x_6(x_5 - w_{HP1})(x_5 - w_{HP2}) - x_5(x_5 + d_{HP})(x_5 + e_{HP}) +$$
$$\rho_{HP}\sin(w_{HP}t) - K_{HP-SA}(x_5 - {x_1}^{T_{dHP-SA}}) - K_{HP-AV}(x_5 - {x_3}^{T_{dHP-AV}}) + u_3 \quad (33)$$

Where $x_i^{\tau} \equiv x_i(t-\tau), and\ \tau$ known as the time delay. Therefore, the mathematical model consists of three coupled oscillators, the ECG signal is formed from the combination of signals as follows (where β is a magnitude scaling factor) [84]:

$$\text{ECG} = (\alpha_0 + \alpha_1 x_1 + \alpha_3 x_3 + \alpha_5 x_5)\beta \quad (34)$$

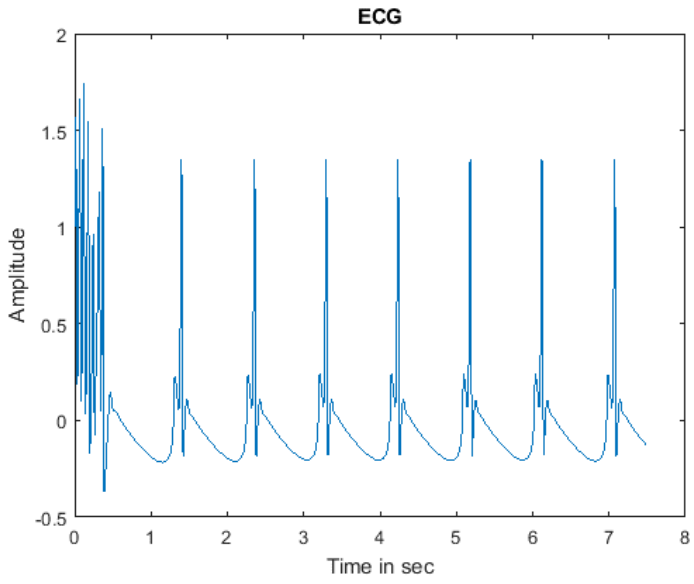

Figure 7 ECG Simulated Equation using Three Coupled Oscillators.

Figure 7 shows the simulated ECG equation, The DDE of the heart model was chosen for modeling the TCD waves. To accomplish that, the cardiac equations were modified to fit the TCD signal:

$$\dot{x}_1 = x_2 \tag{35}$$

$$\dot{x}_2 = -3x_2(x_1 - 0.2)(x_1 + 1.9) - x_1(x_1 + 3)(x_1 + e_{SA})) \tag{36}$$

$$\dot{x}_3 = x_4 \tag{37}$$

$$\dot{x}_4 = -a_{AV}x_4(x_3 - 0.1)(x_3 + 0.1) - x_3(x_3 + 3)(x_3 + 3) - 5(x_3 - x_1{}^{T_{lag\ value\ 1}}) \tag{38}$$

The parameters that were chosen for the model are summarized in the Table 1.

Table 1. TCD envelope DDE parameters

	Parameter
Lag Value	0.8
Initial Values	0, 0.7, 0, 0.2
a_{SA}	3
w_{SA1}	0.2
w_{SA2}	-1.9
d_{SA}	3
w_{AV1}	0.1
w_{AV2}	-0.1
d_{AV}	3
e_{AV}	3
a_{HP}	5
w_{HP1}	1
w_{HP2}	-1
d_{HP}	3
e_{HP}	7

K_{HP-AV}	20

The TCD spectral envelope is modeled by the linear transform:

$$TCD\ envelope = \beta x_3 + \alpha_0 \quad (39)$$

This value is clipped at specific threshold. The parameters $\alpha_0, \beta, e_{SA}, a_{AV}$ and the threshold are the only parameters to be tuned in our model.

Adaptive Medication Pump

Syringe injection pumps are used for treatment using slow medications injection or for injection plasma to the blood. Any syringe injection pump consists of three essential parts; fluid bag, clamp and hook [87]. The fluid is fixed with gears and roller, when the roller rotates, the gear will move then the fluid transfers to patient. The user should define the fluid flow and the required volume. The tube contains an air detector sensor to sense the occurrence of air bubbles, and there is another sensor, which is Pressure sensor to sense any excessive injection pressure. So, these sensors are connected to alarm to inform the user that something wrong has happened. The speed and accuracy of injection with a given amount of drug at predetermined time are very important for cerebrovascular patients without human assistance. There are two factor that control the rate of injection; the syringe diameter and the defined flow rate. The high or even the low injection dosages can be dangerous for patients. The measurement units are milliliters per hour(mL/h). The first attempt of automatic syringe pump was in 1492 [87]. Then, this branch was progressed slowly until in 1658, Christopher Ren produced the first injection device. After that these experiments led to patient's death. The syringe production was stopped due to patient's

death. In 20th century, the plastic bags were replaced with empty bottles which reduced the presence of air. In 1970, Dean Came invented the first injection pump that connected to the patient during movement for treatment, this device helps the diabetic patients who needed injections at certain times [87].

An Arduino-Uno microcontroller board can be used to control the stepper motor which is attached with syringe pump. The Arduino can be connected to liquid crystal display (LCD) and Keypad also to the separate power supply should supply stepper motor to avoid damage the controller from over current of the stepper motor. For the moving mechanism, the stepper motor moved the slider to infuse or diffuse the syringe. Motor driver (L293D) is controlled by Arduino for sending signal to stepper motor.

CHAPTER 3

RESULTS AND DISCUSION

In this study, we used the machine learning for classifying unlabeled novel TCD signals and the obtained results are compared to a manual expert classification.

A supervised learning approach was used to train the classifier. We can enhance the efficiency of the algorithm by increasing the number of training information and the number of extracted features. The goal of supervised machine learning is to extract the model that makes an estimation based on evidence in the known input data and known output. Then, this model can predict the future output data. It is complicated to extract the correct model which is based on trial and error technique, for example, when the model has too many parameters to train, the training data will generate a sensitive model that will model minor variation which can be noise. On the other, hand too simplistic model will have low classification accuracy. Therefore, the right algorithm is a tradeoff between the training data, the number of features, accuracy, model speed, and complexity. The following schematic in Figure 8 helps to overcome some of the machine learning challenges.

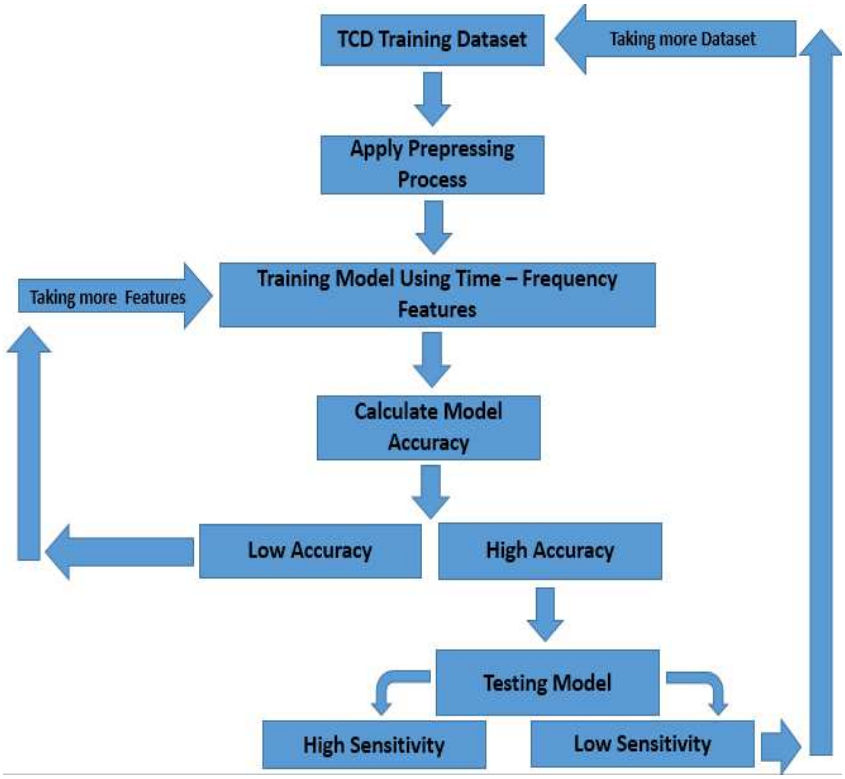

Figure 8 Machine Learning Framework.

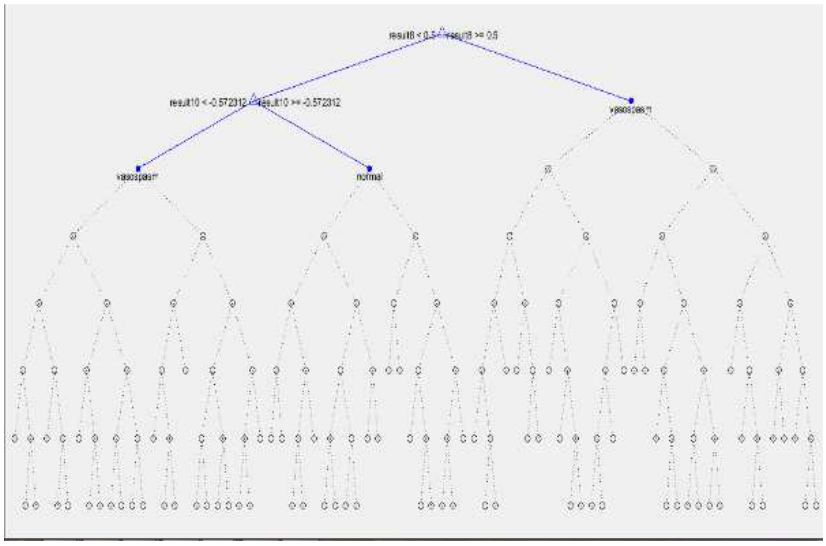

Figure 9 Two out of 34 Levels are Shown in Decision Tree.

First, use preprocessing processes like data scaling and normalization to standardize the values, after that use a certain number of time-frequency features, and then apply the classifier. If the model accuracy after training the dataset is low, so we should increase the

number of features. When we get a high detection accuracy, then, we should start testing the extracted model by using testing datasets. If the sensitivity of the model is low, so we should take more training dataset in the beginning. This loop should be repeated until we reach high accuracy and sensitivity model for the detection.

The Extracted CV Model

In the example of cerebral vasospasm detection, we used 12 time-frequency features to extract a high sensitivity model with using a decision tree classifier. The decision tree contains branches and leaves, where the decision rule can be made by an if conditional statement. Figure. 9 shows an example of two levels out of 34 levels of our decision tree classifier.

We addressed overfitting by limiting the training-set size to 12 files and minimized underfitting by increasing the number of features. In our work, we extracted the classifier training model from two sets of six doppler audio files each side (RMCA and RMCA), one from vasospastic vessels, and the other without CV. The features described above were extracted and used for training.

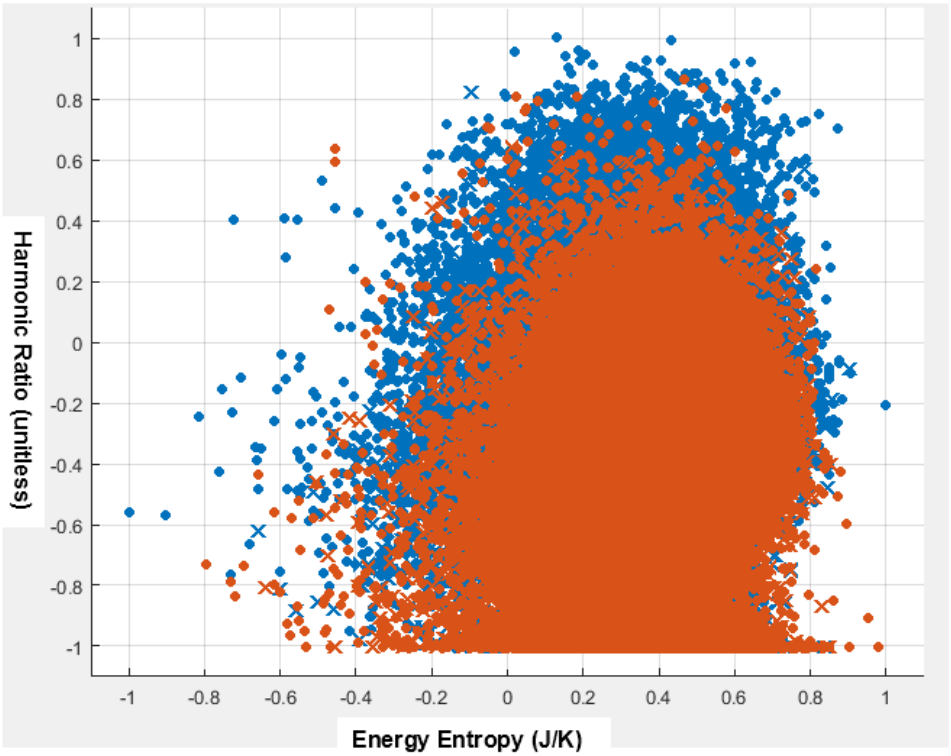

Figure 10 Scatter Plot of Energy Entropy and Harmonic Ratio in the Training Model.

We extracted the bagged trees model, which yielded overall 89.17% accuracy for 160 TCD signals (Normal and CV cases). The system classifies the audio files into normal or CV. Figure 10 is the scatter plot between the two features (energy entropy and harmonic ratio). Figure 11 shows the relation between spectral entropy and harmonic ratio. The confusion matrix in Figure 12 shows that 89.74% cases are predicted correctly as normal (true negative rate) and 87.5% are predicted correctly as CV (true positive rate). On the other hand, the false positive rate is 12.5% and false negative rate 10.26% (where green diagonal is the correctly predicted samples, and the pink diagonal is the confused ones).

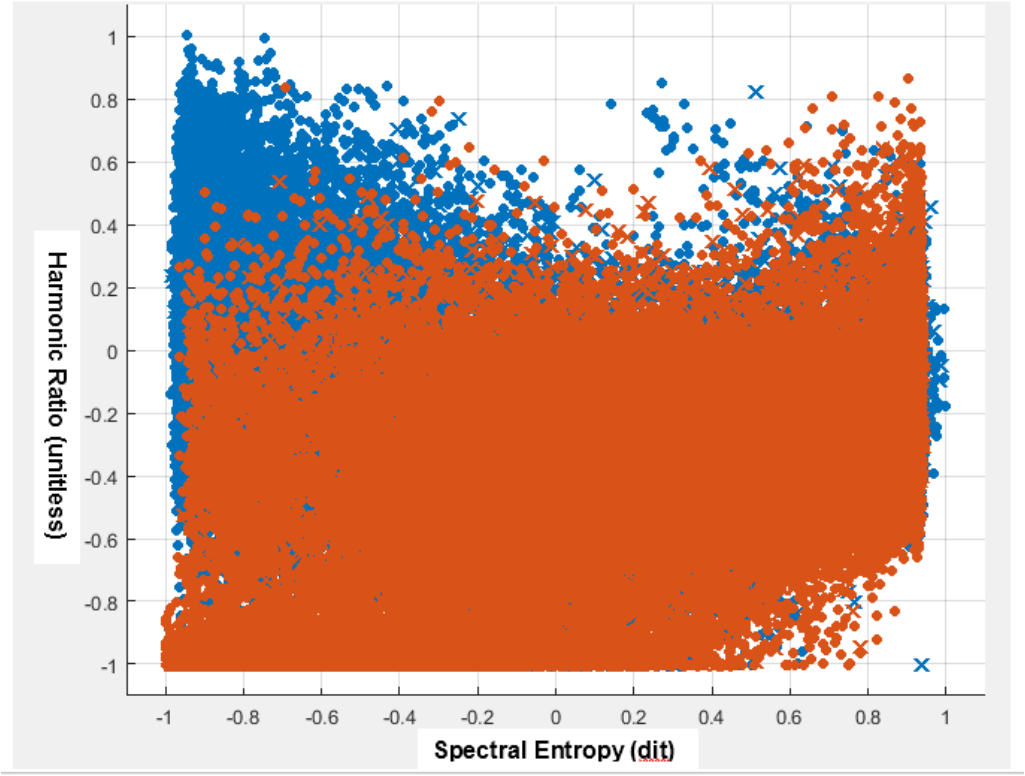

Figure 11 Scatter Plot of Spectral Entropy and Harmonic Ratio in the Training Model.

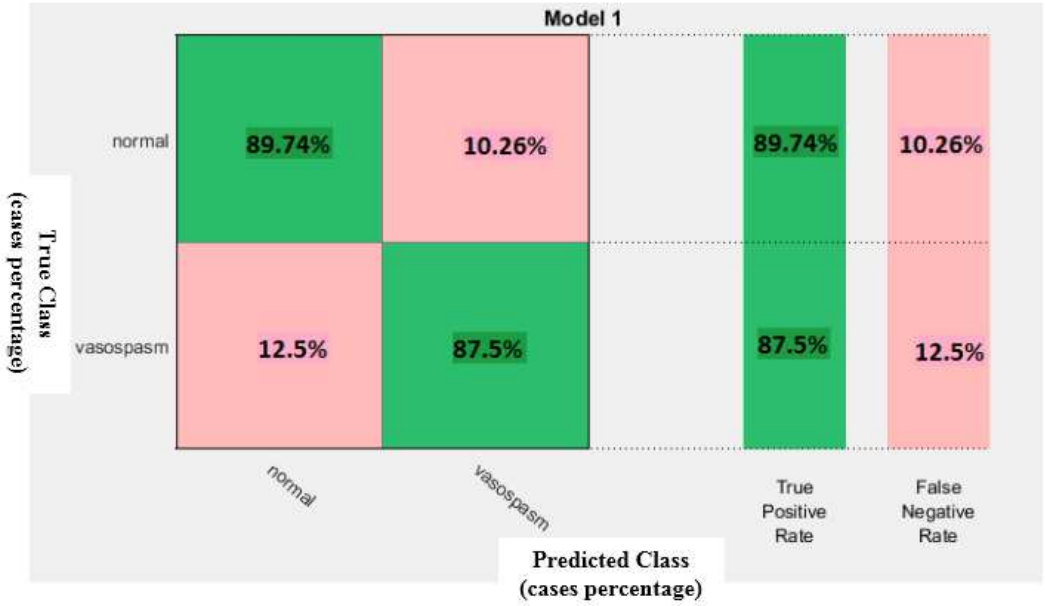

Figure 12 The Confusion Matrix of Decision Tree Matrix in Two Cases.

Error analysis was performed using Precision and Recall measures:

Precision=$\frac{tp}{tp+fp}$

Recall= $\frac{tp}{tp+fn}$

where tp is true positive, fp is false positive, and fn is false negative. Precision is the relation between the true positive and the number of predicted positive (true positive and false positive) which equaled 87.5%. This shows what fraction actually has CV. The recall value is the relation between true positive and the number of actual positive (true positve and false negative) which equaled 89.5% and shows what fraction was correctly detected as having CV. There is a trade-off between the recall and precision [88].

Error analysis was also measured by Receiver operating characteristic (ROC), which is a statistical graphical plot that shows the efficiency of a binary classifier, where the true positive curve is called probability of detection and the false negative rate is the probability of false alarm. The result for our model is shown in Figure 13.

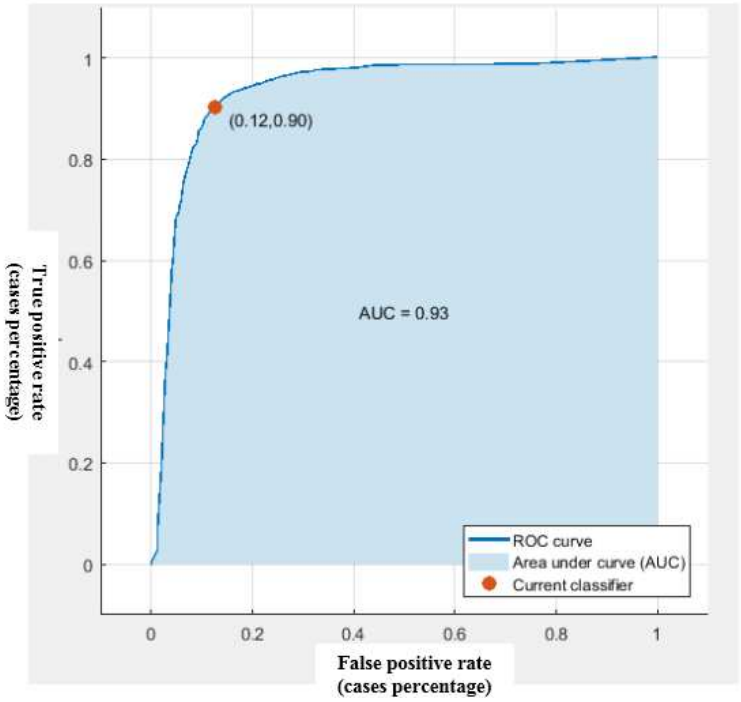

Figure 13 ROC for Decision Tree Classifier.

Firstly, we should test the efficiency and evaluate the success of the proposed algorithm that is based on 12 features. The 12 features were added and the results are calculated in terms of sensitivity, specificity, and accuracy using the decision tree classifier. The main now is to test the influence of noise on the tested dataset. The experimental results of 160 wave files with the bagged decision tree classifier are 87.5% for sensitivity and 89.77% for specificity, but all these results without adding any type of noise to signal.

It is important to note that normal signal might produce false alarms that could be resolved using standard filering techniques of signal averaging over long enough intervals. Since the onset of CV might take many minutes, that kind of time averaging is appropriate. In presence of moderate CV, the developed algorithm could misdetect the CV, but again time averaging corrects that behavior. This result emphasizes that the CV degree is very important for the monitoring and treatment.

Robustness to Noise Test for the Developed Model

In the TCD device, Power M-mode program is built-in TCD. It can simulate the velocity of blood in RMCA, LMCA, and Basial artery (BA) with calculating its power, the number of samples, mean, DIAS (Desmoteplase (chemical compound) in Acute Stroke) and PI (pulsatility index is calculated by peak systolic velocity-end diastolic velocity)/time averaged velocity**)**. This can be shown in Figure 3. After that, the recorded wave file is taken from TCD to MATLAB to confirm signal processing on wave file and then to detect the patient in normal case or CV. Figure 15 shows the signal before training and testing by machine learning.

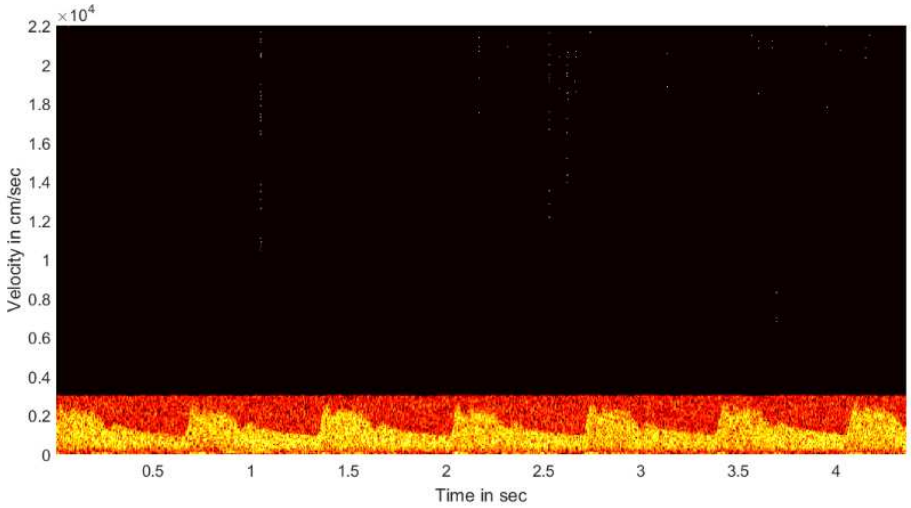

Figure 14 Simulated TCD Signal Before Appling Machine Learning Step.

So, it is important to study the robustness to noise on the dataset with different noise power. Figure 16 shows the evaluation of the proposed model to noise robustness, by adding the Additive White Gaussian noise (AWGN) to the dataset. The experiments show that the CV detection model is robust to noise until 30 SNR and in the normal detection until 60 SNR. This AWGN can yield from the TCD cable, power line or TCD probes.

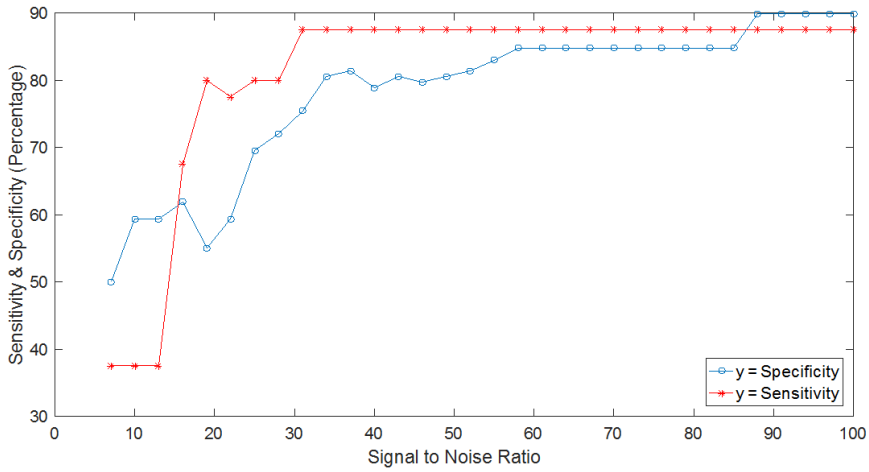

Figure 15 SNR with Sensitivity and Specificity Percentage.

Enhancing the Model by Using the Wavelet Features

After that, we used the wavelet transform features for enhancing the classifier efficiency in addition to using the 12 features described before. CWT was found to be better than DWT in distinguishing between the signals. The wavelet coefficients were applied using the Morlet wavelet. Figure 17,18 show the CWT coefficients for the normal and CV participants, respectively, where the x-axis represents time position along the wave file, the y-axis is the wavelet coefficient or scale (from 1 to 64, high scale means stretched wavelet and slowly changed signal with low frequency) and the color scale reflects the magnitude of each coefficient (the dark color means the lower magnitude and the bright the higher).

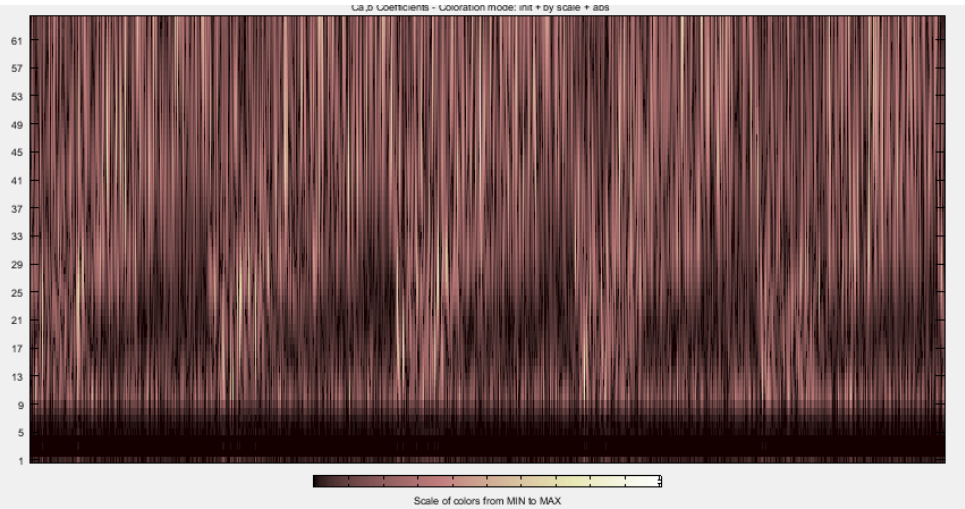

Figure 16 Wavelets Coefficients for Normal Subject.

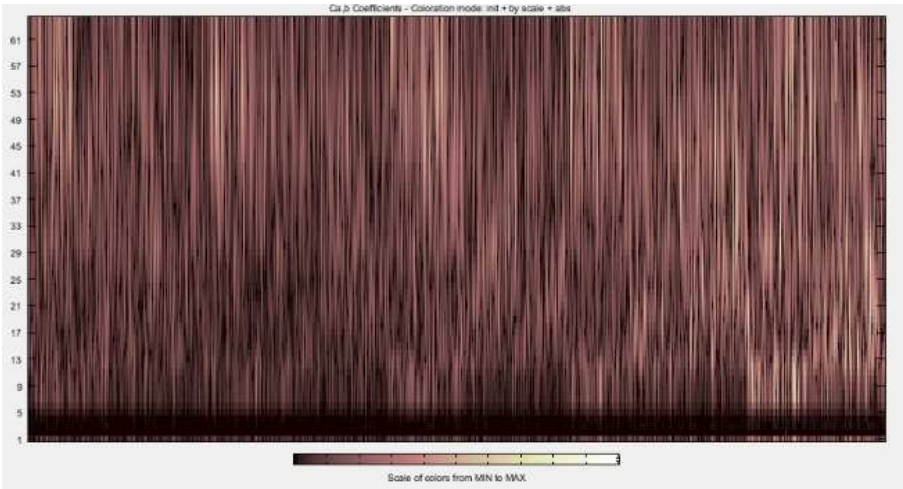

Figure 17 Wavelets Coefficients for CV Subject.

At this stage, to test the efficiency and evaluate the success of the proposed algorithm that based on 12 features and CWT coefficients. Firstly, one by one feature was added and every time the results are calculated in terms of sensitivity, specificity, and accuracy. The main purpose is to test the influence of each feature on the tested dataset. The experimental results of 160 wave files with bagged decision tree classifier are summarized in the Table 2. The 12 features with bagged decision tree classifier give the experimental results are 87.5% sensitivity and 89.77% for specificity.

After that, wavelet technique is applied to reduce the false alarm detection in positive and negatives subjects; the highest accuracy is obtained with 92.5% sensitivity and 95% specificity.

As seen in the Table 3, the proposed model is compared by using various classifiers which are applied to the same dataset. The performance of the classifiers is evaluated using sensitivity, specificity, and accuracy. Decision tree and KNN give us the same accuracy, but KNN has high specificity percentage, on the other hand, bagged decision tree gives the highest in sensitivity percentage.

Table 2 The Performance of Bagged Decision Tree with Adding Different Features.

Table 2- Bagged Decision Tree Classifier Performance			
Adding Features	**Sensitivity (%) (CV)**	**Specificity (%) (Normal)**	**Accuracy (%)**
Zero Crossing	51.7	92.5	62
Energy	78.8	67.5	75.94
Energy Entropy	77.9	67.5	75.31
Spectral Centroid	83.9	65	79.11
Spectral Spread	83.9	67.5	79.74
Spectral Entropy	88.9	77.5	86

Spectral Flux	89.8	80	87.34
Spectral Roll off	77.9	92.5	81.64
MFCC	80.5	92.5	83.5
Harmonic Ratio	83	97.5	86.7
First Chroma	84.7	92.5	86.7
Second Chroma	89.83	87.5	89.24
CWT	95	92.5	93.7

Table 3 Comparison of the Performance of Different Classifiers.

Table 3 – **Comparison** Between Different Classifiers			
Classifier	**Sensitivity (%) (CV)**	**Specificity (%) (Normal)**	**Accuracy (%)**
Bagged Decision Tree	89.83	87.5	89.24
Linear Decimator	55.9	95	65.82
KNN	91.52	85	89.87
Logistic Regression	44.9	92.5	56.9

Representative spectrograms of three groups are shown in Fig. 19-22. The blue envelope curves are the result of a modeling using DDE and the red/yellow spectrograms are obtained from the participants. The envelopes in all cases have different cycle duration, the highest horizontal level and the lowest horizontal level. Table 4 shows the statistics of the TCD signal extrema levels and cycle durations.

Table 4. TCD Signal Statistics

Signal Specification	Cycle Duration Min	Cycle Duration Max	Max value for Highest Level	Min value for Highest Level	Max value for Lowest Level	Min value for Lowest Level
Control	0.6	1	3094	1504	1418	515.6
CV	0.65	1.18	6016	3652	2874	1848

In order to obtain the features of the normal, hyperemia and CV cases, samples from each case are taken. Based on the equation (39), it was observed that there was a certain range for variable values for each group. There are four variables that should be set $(e_{SA}, a_{AV}, \alpha_0, \beta)$ and other parameters kept constant, so we can estimate the CBFV in the three cases. The e_{SA} values represent the cycle rate of the brain middle artery , a_{AV} value represents the width of positive cycle of the brain middle artery, α_0 value represents the DC signal offset value from the x axis and β value represents the scale. Table 5 summarizes average values that are appropriate for three groups of interest.

Table 5. DDE Model Typical Parameters

Cases	Normal Case	Hyperemia Case	Cerebral Vasospasm Case
e_{SA}	5.2	5.5	4.66
a_{AV}	7	3	5
α_0	4150	8500	13000
β	1600	2850	4150

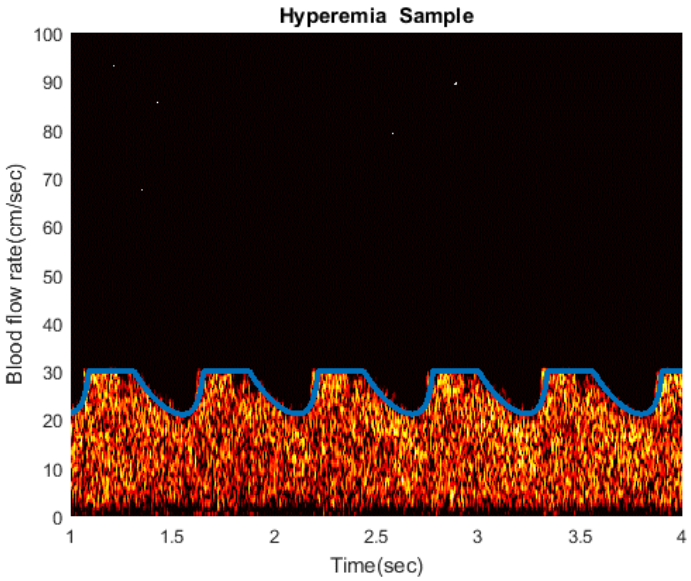

Figure 18 Graphical Comparison between the Real TCD Signal and Modelled One in the Hyperermia Case.

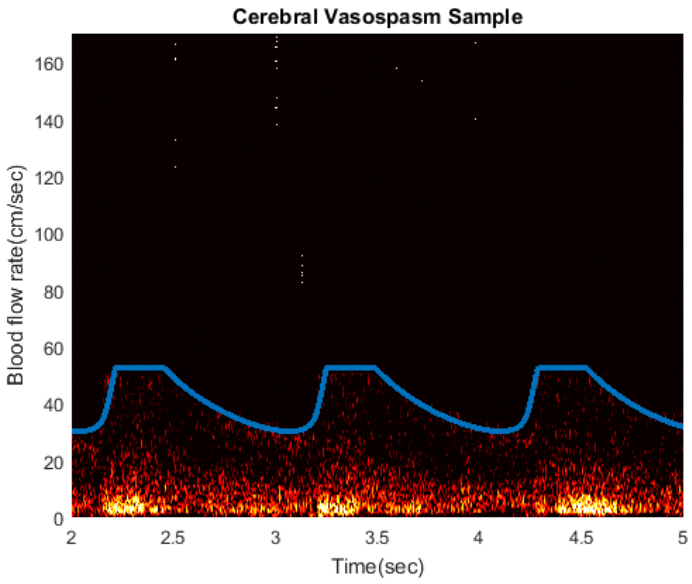

Figure 19 Graphical Comparison Between the Real TCD Signal and Modelled One in the Cerebral Vasospasm Case.

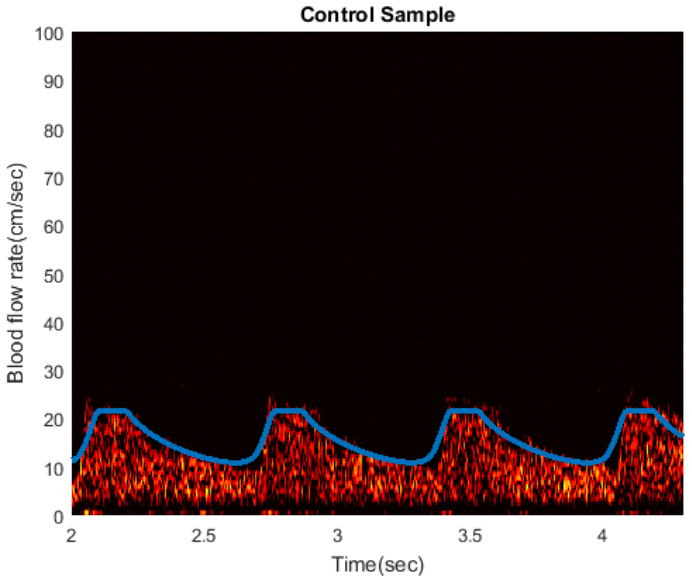

Figure 20 Graphical Comparison Between the Real TCD Signal and Modelled One in the Normal Case.

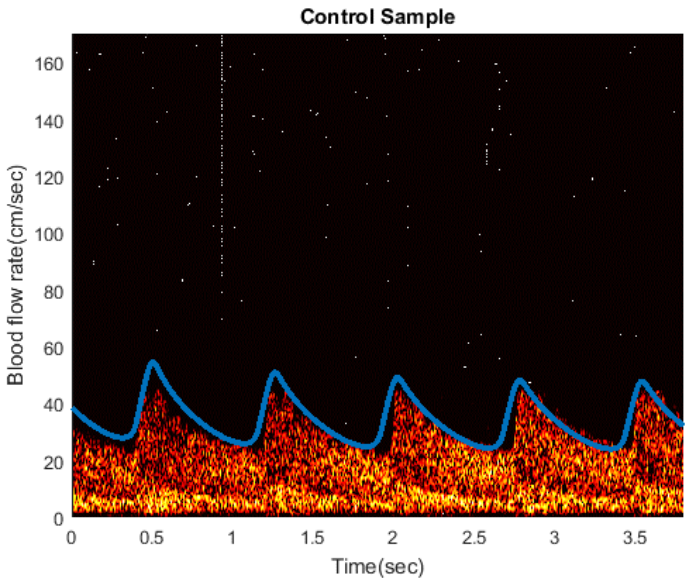

Figure 21 Graphical Comparison Between the Real TCD Signal and Modelled One in the Normal Case.

Based on equation (39), we could generate many TCD signals. To validate this model, a validation waves (2 control cases, 1 Hyperemia and 1 CV case) were selected from TCD datasets. Figure 19,20,21,22 show the difference between the real TCD signal and the extracted DDE model in Hyperemia, CV and normal respectively. The results show good fit to the envelope of the real signals.

We have found that by changing four parameters in the proposed delay differential equations, we could transfer from one case to another. The DDE achieved highly efficient output close to the original TCD output. These equations can be used widely in neurological studies of a cerebral hemodynamics. The mathematical model of TCD signal can significantly improve and modernize the understanding of the undergoing processes.

Unfortunately, not all TCD recording spectrums are clean and high contrast and the predication performance directly depends on the quality of a signal and noise level. More precise ranges of parameter could be extracted for the model after obtaining more high quality TCD data.

CV Treatment with Medical Pump Control

The second part of the study is to present an algorithm for medication controlling along the pump for CV treatment. We will use a developed algorithm for controlling medication in the blood using a closed-loop infusion pump.

The prototype mechatronic syringe pump consists of a keypad, LCD and stepper motor. The stepper motor starts to rotate at pre-programmed time with given speed. Arduino was used to control the stepper motor. T was the time for a single stepper motor pulse, T_i' was the time of motor pulses that required in i^{th} experiment and P_i was the estimated number of pulses in i^{th} experiment. By experiments, P_i pulses generated CC_i. The following can be used for determining the number of pulses P_i in i^{th} experiment

$$P_i = \frac{T_i'}{T}$$

P_F was defined as the number of stepper motor pulses for the full syringe injection (CC_F), therefore it can be predicted by:

$$P_F = \frac{\sum \frac{P_i * CC_F}{CC_i}}{Number\ of\ experiments}$$

The stepper motor velocity for i^{th} experiment can be measured by:

$$V_i = \frac{CC_{i+1} - CC_i}{T_{i+1} - T_i}$$

Therefore,

$$\text{The average motor velocity} = \frac{\sum V_i}{Number\ of\ experiments}$$

The frequency required to enable the motor is reciprocal the time of each step

$F = \frac{1}{T}$.

There are many techniques for drive and control the syringe pump. We will use the controller with the open source microcontroller board (Arduino) to regulate the pressure in the syringe. This technique offers a low-cost option to drive and control the pressure in the syringe. The syringe pump is the most commonly used as a device that maintain more stable flows than recirculation pumps and peristaltic with easy to setup and use. Our syringe pump system is consisting of four essential parts: the syringe pump, pressure sensor, microcontroller, the stepper motor and the stepper driver. Figure 22 shows the system layout. The syringe pump used to offer the certain displacement for forcing the medication. The pressure sensor (piezoresistive pressure) used to continuous monitoring the pressure inside the pump. The Arduino microcontroller board is taking the reading from the pressure sensor and then controlling the motor driver while increasing or decreasing the pressure.

To control pressure in the pump, we used the controller which has a highly responsive and stable. The controller can be used to optimize the pressure response to fit a certain application. In biomedical field, pressure overshot can cause problems. So, the derivative gain is used to prevent this overshooting, but it has a disadvantage of longer response time.

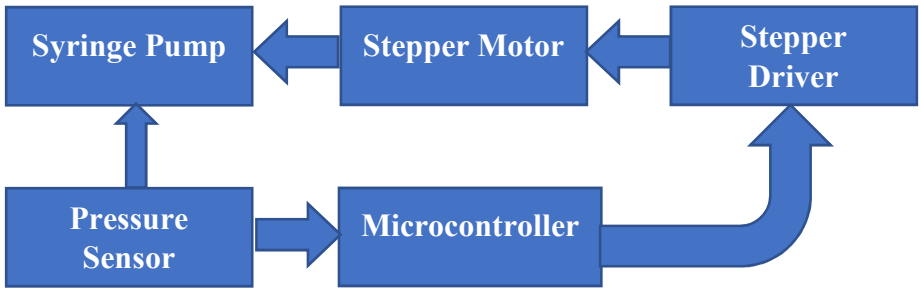

Figure 22 Syringe pump controller layout.

CONCLUSION AND FUTURE WORK

Novel algorithm for CV detection, based on audio and music signal analysis of TCD spectra, was developed using supervised machine learning framework. Time and frequency features were extracted from the signal, and they were used as input to the ensemble decision tree classifier. This CV detection research algorithm was tested against the noise by using 12 features with ensemble bagged decision tree. This classifier produced robust detection of CV with over 87.5% success rate and 92.5% for normal and can be applied in real time. Then we used the wavelets for expanding the feature set and to enhance the accuracy detection. It is shown that CWT gives a high detailed description of the normal and CV blood flow rate sound cases, where this method monitored the time, frequency and shape in details. When the developed algorithm was tested the classification efficiency performance are 92.5% sensitivity and 95% specificity. Our autonomous CV detector can allow development of continuous vasospasm monitoring with automatic alarming on this dangerous condition in both clinically and for cerebrovascular research and with decreasing the physician's attendance in the neurology clinics.

The observation of the experimental data clarifies there is a high relationship between cardiac waves which is taken by electroencephalogram (EEG) and CBFV waves of the brain which is taken by TCD especially in ST interval. In this study, we share a curious

observation that the mathematical models that were developed for modeling cardiac waves could be modified and applied to a cerebral blood velocity flow modeling. Our results show that various behaviors of TCD signal spectrum could be precisely modeled with delay differential equations that build a model with only 4 parameters. Our approach (model) uses routinely TCD signals which are wave files, does not require any training on TCD data before using, does not need calibration, and is applicable across a large range of patients. The fitting process works well with high resolution spectrogram but it could fail with the low-resolution or low-quality spectrograms. We proposed an intuitive way to tune those parameters to fit the model to the real TCD data recorded in clinic.

We successfully applied the model to demonstrate the differences between three groups of signals: CV, hyperemia and control. In the future this model could potentially help in earlier detection of CV, but its main benefit that it could be applied to other disorders related to cerebral blood flow and could improve understanding of the mechanisms involved in the process. These equations can be used widely in neurology studies of a cerebral hemodynamics in various vascular problems. A syringe pump system has been used to supply an automatic process for flow control of medication. We have presented a device that injects certain amount of cc of drug into the patient in a prescribed time.

In the future research, one could try to use the classifier decision output and design embedded on real-time system for treatment purposes, along controlling pump medication to restore the cerebral blood flow to its normal state. It would be desirable to develop an algorithm for CV prediction before it happens.

LIST OF REFERENCES

[1] [Online]. Available: http://www.strokecenter.org/patients/about-stroke/stroke-statistics..

[2] G. Tsivgoulis and . A. Alexandrov, "Cerebral hemodynamics in acute stroke: pathophysiology and clinical implications," *Journal of Vascular and Interventional Neurology,* vol. 1, no. 3, pp. 65-69, 2008.

[3] N. W. C. Dorsch, "Cerebral arterial spasm--a clinical review," *British Journal of Neurosurgery,* vol. 9, no. 3, pp. 403-12, 1995.

[4] J. M. Wardlaw and e. al., "Is routine transcranial Doppler ultrasound monitoring useful in the management of subarachnoid hemorrhage?," *Neurosurg,* vol. 88, no. 2, pp. 272-6, 1998.

[5] R. Aaslid, P. Huber and H. Nornes, "A transcranial Doppler method in the evaluation of cerebrovascular spasm," *Neuroradiology,* vol. 28, no. 1, pp. 11-16, 1986.

[6] S. J. Michael and e. al., "Frequency and clinical impact of asymptomatic cerebral infarction due to vasospasm after subarachnoid hemorrhage," *Journal of Neurosurgery,* vol. 109, no. 6, pp. 1052-1059, 2008.

[7] [Online]. Available: http://clinicalgate.com/stroke-8/.

[8] [Online]. Available: https://en.wikipedia.org/wiki/Basilar_artery.

[9] G. Kumar, R. B. Shahripour and . M. R. Harrigan, "Vasospasm on transcranial Doppler is predictive of delayed cerebral ischemia in aneurysmal subarachnoid hemorrhage: a systematic review and meta-analysis," *Neurosurgery,* vol. 124, no. 5, pp. 1257-64, 2015.

[10] E. S. Connolly and e. al., "Guidelines for the management of aneurysmal subarachnoid hemorrhage: a guideline for healthcare professionals from the American Heart Association/american Stroke Association.," *Stroke,* vol. 43, no. 6, pp. 1711-37, 2012.

[11] S. TF and e. al., "Evidence-based guideline: clinical evaluation and treatment of transverse myelitis: report of the Therapeutics and Technology Assessment Subcommittee of the American Academy of Neurology," *Neurology,* vol. 77, no. 24, pp. 2128-34, 2011.

[12] D. MN and e. al., "Critical care management of patients following aneurysmal subarachnoid hemorrhage: recommendations from the Neurocritical Care Society's Multidisciplinary Consensus Conference.," *Neurocrit Care,* vol. 15, no. 2, pp. 211-40, 2011.

[13] G. Kumar and e. al., "Trends in transcranial doppler monitoring in aneurysmal subarachnoid hemorrhage: A 10-Year analysis of the nationwide inpatient sample," *Journal of Stroke and Cerebrovascular Diseases,* vol. 26, no. 4, pp. 851-857, 2016.

[14] D. Evans, W. McDicken, R. Skidmore and J. Woodcock, Doppler Ultrasound: Physics, Instrumentation, and Clinical Applications, John Wiley and sons, 1989.

[15] P. Hoskins, "Measurement of arterial blood flow by Doppler ultrasound.," *Clin Phys Physiol Meas.,* vol. 11, no. 1, pp. 1-26, 1990.

[16] R. Ganpath, "Doppler ultrasound technique used to determine the blood," 2006.

[17] [Online]. Available: http://spencertechnologies.com/products.html.

[18] C. Lodi and M. Ursino, "Hemodynamic effect of cerebral vasospasm in humans: A modeling study," *Annals of Biomedical Engineering,* vol. 27, no. 2, pp. 257-273, 1999.

[19] G. Mader, M. Olufsen and A. Mahdi, "Modeling cerebral blood flow velocity during orthostatic stress," *Annals of Biomedical Engineering,* vol. 43, no. 8, pp. 1748-1758, 2015.

[20] M. Li, H. Huang, M. L. Boninger and E. Sejdić, "An analysis of cerebral blood flow from middle cerebral arteries during cognitive tasks via functional transcranial Doppler recordings," *Neuroscience Research,* vol. 84, pp. 19-26, 2014.

[21] İ. Güler, F. Hardalaç and M. Kaymaz, "Comparison of FFT and adaptive ARMA methods in transcranial Doppler signals recorded from the cerebral vessels.," *Computers in Biology and Medicine,* vol. 32, no. 6, pp. 445-453, 2002.

[22] A. Ozturk and A. Arslan, "Classification of transcranial Doppler signals using their chaotic invariant measures," *Computer Methods and Programs in Biomedicine,* vol. 86, no. 2, pp. 171-180, 2007.

[23] H. Uğuz, "A hybrid system based on information gain and principal component analysis for the classification of transcranial Doppler signals," *Computer Methods and Programs in Biomedicine,* vol. 107, no. 3, pp. 598-609, 2012.

[24] S. Valle, W. Li and S. J. Qin, "Selection of the number of principal components: The variance of the reconstruction error criterion with a comparison to other methods," *American Chemical Society,* vol. 38, no. 11, p. 4389–4401, 1999.

[25] L. Ferré, "Selection of components in principal component analysis: A comparison of methods," *Computational Statistics & Data Analysis,* vol. 19, no. 6, pp. 669-682, 1995.

[26] M. Awad and Y. Motai, "Dynamic classification for video stream using support vector machine," *Applied Soft Computing,* vol. 8, no. 4, pp. 1314-1325, 2008.

[27] A. Ozturk, A. Arslan and F. Hardalac, "Comparison of neuro-fuzzy systems for classification of transcranial Doppler signals with their chaotic invariant measures," *Expert Systems with Applications,* vol. 34, no. 2, pp. 1044-1055, 2008.

[28] H. Uğuz, A. Öztürk, R. Saraçoğlu and A. Arslan, "A biomedical system based on fuzzy discrete hidden Markov model for the diagnosis of the brain diseases," *Expert Systems with Applications,* vol. 35, no. 3, pp. 1104-1114, 2008.

[29] H. Uğuz and A. Arslan, "A new approach based on discrete hidden Markov model using Rocchio algorithm for the diagnosis of the brain diseases," *Digital Signal Processing,* vol. 20, no. 3, pp. 923-934, 2010.

[30] J. Ryu, N. Ko, X. Hu and S. Shadden , "Numerical investigation of vasospasm detection by extracranial blood velocity ratios," *Cerebrovascular Diseases,* vol. 43, pp. 214-222, 2017.

[31] V. Bruni and D. Vitulano, "Combined image compression and denoising using wavelets," *Signal Processing: Image Communication,* vol. 22, no. 1, pp. 86-101, 2007.

[32] J. Chen, Y. Zhang and X. Shi, "Image coding based on wavelet transform and uniform scalar dead zone quantizer," *Signal Processing: Image Communication,* vol. 21, no. 7, pp. 562-572, 2006.

[33] J.-D. Wu and C.-C. Hsu, "Fault gear identification using vibration signal with discrete wavelet transform technique and fuzzy–logic inference," *Expert Systems with Applications,* vol. 36, no. 2, pp. 3785-3794, 2009.

[34] S. Ekici, S. Yildirim and M. Poyraz, "Energy and entropy-based feature extraction for locating fault on transmission lines by using neural network and wavelet packet

decomposition," *Expert Systems with Applications,* vol. 34, no. 4, pp. 2937-2944, 2008.

[35] İ. Güler and E. Übeylı˙, "ECG beat classifier designed by combined neural network model," *Pattern Recognition,* vol. 38, no. 2, pp. 199-208, 2005.

[36] L. Ferini-Strambi, A. Walters and D. Sica, "The relationship among restless legs syndrome (Willis–Ekbom Disease), hypertension, cardiovascular disease, and cerebrovascular disease," *Journal of Neurology,* vol. 261, no. 6, pp. 1051-1068, 2014.

[37] K. Kienreich and e. al, "Vitamin D, arterial hypertension & cerebrovascular disease," *Indian Journal of Medical Research,* vol. 137, no. 4, pp. 669-679, 2013.

[38] P. Berg and e. al., "Cerebral blood flow in a healthy Circle of Willis and two intracranial aneurysms: computational fluid dynamics versus four-dimensional phase-contrast magnetic resonance imaging.," *Journal of Biomechanical Engineering,* vol. 136, no. 4, pp. 13-1247, 2014.

[39] Y.-J. Lee, Y.-C. Rhim, M. Choi and T.-S. Chung, "Validation of compliance zone at cerebral arterial Bifurcation Using Phantom and computational fluid dynamics simulation," *Journal of Computer Assisted Tomography,* vol. 38, no. 3, pp. 480-484, 2014.

[40] M. Olufsen, . A. Nadim and . L. Lipsitz, "Dynamics of cerebral blood flow regulation explained using a lumped parameter model," *American Journal of Physiology,* vol. 282, no. 2, pp. R611-R622, 2002.

[41] M. Ursino, "Mechanisms of cerebral blood flow regulation," *Critical Reviews in Biomedical Engineering,* vol. 18, no. 4, pp. 255-288, 1991.

[42] M. Neidlin, U. Steinseife and T. Kaufmann, "A multiscale 0-D/3-D approach to patient-specific adaptation of a cerebral autoregulation model for computational fluid dynamics studies of cardiopulmonary bypass," *Journal of Biomechanics,* vol. 47, no. 8, pp. 1777-1783, 2014.

[43] J. Russin, H. Babiker, J. Ryan and e. al., "Computational Fluid Dynamics to Evaluate the Management of a Giant Internal Carotid Artery Aneurysm," *World Neurosurgery,* vol. 83, no. 6, pp. 1057-1065, 2015.

[44] B. Liu and e. al., "A non-invasive method to assess cerebral perfusion pressure in geriatric patients with suspected cerebrovascular disease," *PLOS ONE,* p. e0120146, 2015.

[45] B. Liu and e. al., "A highly similar mathematical model for cerebral blood flow velocity in geriatric patients with suspected cerebrovascular disease," *Scientific Reports,* vol. 5, p. 15771, 2015.

[46] S. Panunzi, L. D'Orsil, D. Iacoviello and A. De Gaetano, "A Stochastic delay differential model of cerebral autoregulation.," *PLos One,* vol. 10, no. 4, p. e011845, 2015.

[47] R. Parker, J. Doyle and J. Harting, "Model predictive control for infusion pump insulin delivery," in *Engineering in Medicine and Biology Society, 1996. Bridging Disciplines for Biomedicine. Proceedings of the 18th Annual International Conference of the IEEE*, Amsterdam, Netherlands, 1996.

[48] R. Hovorka and e. ai., "Nonlinear model predictive control of glucose concentration in subjects with type 1 diabetes," *Physiological Measurement,* vol. 25, no. 4, 2004.

[49] R. Parker, F. Doyle and N. Peppas, "A model-based algorithm for blood glucose control in Type I diabetic patients," *IEEE Transactions on Biomedical Engineering,* vol. 46, no. 2, pp. 148 - 157, 1999.

[50] K. Umapathy, S. Krishnan and R. Rao, "Audio signal feature extraction and classification using local discriminant bases," *IEEE Transactions on Audio, Speech, and Language Processing,* vol. 15, no. 4, pp. 1236 - 1246, 2007.

[51] G. Tzanetakis and P. Cook, "Musical genre classification of audio signals," *IEEE Transactions on speech and audio processing,* vol. 10, no. 5, pp. 293-302, 2002.

[52] M. Xu, N. Maddage and C. Xu, "Multimedia and Expo, 2003. ICME '03. Proceedings.," in *Creating audio keywords for event detection in soccer video*, Baltimore, MD, USA, 2003.

[53] R. Schafer and L. Rabiner, An Introduction to Digital Speech Processing (Foundations and Trends in Signal Processing,), Foundations and Trends in Signal Processing,, 2007.

[54] H. Kim, N. Moreau and T. Sikora, Audio and Beyond: Audio Content Indexing and Retrieval MPEG-7, John Wiley & Sons, 2005.

[55] T. Zhang and C. Kuo, "Audio content analysis for online audiovisual data segmentation and classification," *: IEEE Transactions on Speech and Audio Processing,* vol. 9, no. 4, pp. 441 - 457, 2009.

[56] . T. Giannakopoulos and A. Pikrakis, Introduction to Audio Analysis: A Matlab Approach., Elsevier, 2014.

[57] O. Lartillot and P. Toiviainen, "A MATLAB toolbox formusicalL feature extraction from audio," in *Proc. of the 10th Int. Conference on Digital Audio Effects (*, France, 2007.

[58] J. Nam, M. Alghoniemy and A. H. T. Tewfik, "Audio-visual content-based violent scene characterization," in *International Conference on Image Processing*, Chicago, IL, USA, 1998.

[59] S. Theodoridis and K. Koutroumbas, "Pattern Recognition and Neural Networks," Springer, 2001, pp. 169-195 .

[60] R. Hasan, . M. Jamil, G. Rabbani and S. Rahman, "Speaker identification using Mel frequency," in *3rd International Conference on Electrical & Computer Engineering*, Dhaka, Bangladesh, 2004.

[61] K. Indrebo, R. J. Povinelli and M. Johnson, "Minimum mean-squared error estimation of mel-frequency cepstral coefficients using a novel distortion model," *IEEE Transactions on Audio, Speech, and Language Processing,* vol. 16, no. 8, pp. 1654 - 1661, 2008.

[62] M. Anusuya and S. Katti , "Mel Frequency discrete wavelet coefficients for kannada speech recognition using PCA," in *Proc. of Int. Conf. on Advances in Computer Science*, 2010.

[63] G. H. Wakefield, "Mathematical representation of joint time-chroma distributions," in *Advanced Signal Processing Algorithms, Architectures, and Implementations* , 1999.

[64] M. Bartsch and G. Wakefield, "Audio thumbnailing of popular music using chroma-based representations," *IEEE Transactions on Multimedia,* vol. 7, no. 1, pp. 96 - 104, 2005.

[65] A. Pikrakis, T. Giannakopoulos and S. Theodoridis, "A speech/music discriminator of radio recordings based on dynamic programming and bayesian networks," *IEEE Transactions on Multimedia,* vol. 10, no. 5, pp. 846 - 857, 2008.

[66] K. Yadati and e. al., "On the automatic identification of music for common activities," in *International Conference on Multimedia Retrieval*, Bucharest, Romania, 2017.

[67] E. Scheirer and M. Slaney, "Construction and evaluation of a robust multifeature speech/music discriminator," in *Acoustics, Speech, and Signal Processing*, Munich, Germany, 1997.

[68] D. Kirovski and H. Malvar, "Spread-spectrum watermarking of audio signals," *IEEE Transactions on Signal Processing,* vol. 51, no. 4, pp. 1020 - 1033, 2003.

[69] C. Sapsanis, G. Georgoulas and A. Tzes, "EMG based classification of basic hand movements based on time-frequency features," in *Control & Automation (MED)*, Chania, Greece, 2013.

[70] H. Shahraki, S. Pourahmad and N. Zare, "K Important Neighbors: A novel approach to binary classification in high dimensional data," *BioMed Research International,* 2017.

[71] H. Frohlich, O. Chapelle and B. Scholkopf, "Feature selection for support vector machines by means of genetic algorithm," in *Tools with Artificial Intelligence, 2003. Proceedings. 15th IEEE International Conference*, Sacramento, CA, USA, 2003.

[72] S. Perkins, K. Lacker and J. Theiler, "Fast, incremental feature selection by gradient descent in function space," *Journal of Machine Learning Research,* vol. 3, pp. 1333-1356, 2003.

[73] J. DaWu and J. MingKuo, "An automotive generator fault diagnosis system using discrete wavelet transform and artificial neural network," *Expert Systems with Applications,* vol. 36, no. 6, pp. 9776-9783, 2009.

[74] H. Ocak, "Automatic detection of epileptic seizures in EEG using discrete wavelet transform and approximate entropy," *Expert Systems with Applications,* vol. 36, no. 2, pp. 2027-2036, 2009.

[75] G. Kumar, K. Elzaafrani and A. Nakhmani, "Machine learning approach to automate detection of cerebral vasospasm using transcranial doppler monitoring,," in *American Academy of Neurology*, Boston, USA, 2017.

[76] M. Signorini and D. Bernardo, "Simulation of heartbeat dynamics: A nonlinear model," *International Journal of Bifurcation and Chaos,* vol. 8, no. 8, 1997.

[77] D. Bernardo and M. Signorini, "A model of two nonlinear coupled oscillators for the study of heartbeat dynamics," *International Journal of Bifurcation and Chaos,* vol. 8, no. 10, 1998.

[78] M. Brandt, G. Wang and H.-T. Shih, "Feedback control of a nonlinear dual–oscillator heartbeat model," *Bifurcation Control,* pp. 265-273, 2003.

[79] . J. C. Sprott, Chaos and Time-Series Analysis.,, Oxford University Press, 2006.

[80] J. Guckenheimer and P. Holmes, Nonlinear Oscillations, Dynamical Systems, and Bifurcations of Vector Fields., Springer, 1983.

[81] G. Frasso, J. Jaeger and P. Lambert, "Estimation and approximation in nonlinear dynamic systems using quasilinearization".

[82] A. Santos, S. Lopes and R. Viana, "Rhythm synchronization and chaotic modulation of coupled Van der Pol oscillators in a model for the heartbeat," *Physica A: Statistical Mechanics and its Applications,* vol. 338, no. 3-4, pp. 335-355, 2004.

[83] S. Gois and M. Savi, "An analysis of heart rhythm dynamics using a three-coupled oscillator model," *Chaos, Solitons & Fractals,* vol. 41, no. 5, pp. 2553-2565, 2009.

[84] S. Gois and M. Savi, "An analysis of heart rhythm dynamics using a three-coupled oscillator model," *Chaos, Solitons & Fractals,* vol. 41, no. 5, pp. 2553-2565, 2009.

[85] S. Campbell and D. Wang, "Relaxation oscillators with time delay coupling," *Physica D: Nonlinear Phenomena,* vol. 111, no. 1-4, pp. 151-178, 1998.

[86] K. Imamasu, H. Suemitsu and C. Matoba, "Parameter estimation of heart rhythm dynamics using adaptive observer," in *Advanced Mechatronic Systems (ICAMechS)*, Kumamoto, Japan, 2014.

[87] M. Jafarzadeh and F. Farokhi, "Design and construction of an automatic syringe injection pump," *Pacific Science Review A: Natural Science and Engineering,* vol. 18, no. 2, pp. 132-137, 2016.

[88] R. Jones, B. Rey, O. Madani and W. Greiner, "Generating query substitutions," in *Proceedings of the 15th International Conference on World Wide Web*, 2006.